Stretto di Messina

Concessionaria per la progettazione, realizzazione e gestione del collegamento stabile tra la Sicilia e il Continente Organismo di Diritto Pubblico
(Legge n° 1158 del 17 dicembre 1971, modificata dal D.Lgs. n°114 del 24 aprile 2003)

EurolinK

PONTE SULLO STRETTO DI MESSINA

PROGETTO DEFINITIVO

EUROLINK S.C.p.A.

IMPREGILO S.p.A. (MANDATARIA)
SOCIETÀ ITALIANA PER CONDOTTE D'ACQUA S.p.A. (MANDANTE)
COOPERATIVA MURATORI E CEMENTISTI - C.M.C. DI RAVENNA SOC. COOP. A.R.L. (MANDANTE)
SACYR S.A.U. (MANDANTE)
ISHIKAWAJIMA - HARIMA HEAVY INDUSTRIES CO. LTD (MANDANTE)
A.C.I. S.C.P.A. - CONSORZIO STABILE (MANDANTE)

IL PROGETTISTA	IL CONTRAENTE GENERALE	STRETTO DI MESSINA	STRETTO DI MESSINA
COWI Ing. E.M. Veje Dott. Ing. E. Pagani Ordine Ingegneri Milano n° 15408 EurolinK	Project Manager (Ing. P.P. Marcheselli)	Direttore Generale e RUP Validazione (Ing. G. Fiammenghi)	Amministratore Delegato (Dott. P. Ciucci)

Unità Funzionale	OPERA DI ATTRAVERSAMENTO	PB0031_F0
Tipo di sistema	STUDI DI BASE	
Raggruppamento di opere/attività	ANALISI GLOBALI	
Opera - tratto d'opera - parte d'opera	Foundation Evaluation	
Titolo del documento	Equivalent Stiffness and Damping Matrices for the Soil-Foundation System, Annex	

CODICE: C G 1 0 0 0 | P | R B | D | P | S B | A 2 | 0 0 | 0 0 | 0 0 | 0 0 | 0 2 | F0

REV	DATA	DESCRIZIONE	REDATTO	VERIFICATO	APPROVATO
F0	20/06/2011	EMISSIONE FINALE	LC	GV	SR/ABI

NOME DEL FILE: PB0031_F0_ANX

INDEX

1 Executive summary

This reports evaluates the equivalent stiffness and damping matrices that should be included in the structural model to represent the deformability and damping of the soil-foundation system in a dynamic analysis of the bridge structure.

The stiffness and damping coefficients are evaluated using solutions provided by Gazetas (1991) for rigid foundations partly or totally embedded in a visco-elastic continuum of finite depth, loaded by harmonic forces.

Since the soil response to seismic loading is non-linear, the secant stiffness and damping must be selected by accounting for the strain level attained during seismic shaking. To this purpose, one-dimensional seismic response analyses were carried out at the sites of the tower foundations and the anchor blocks of the Messina bridge.

The seismic input included the acceleration time-histories presented in Document DT/ISP/S/E/R1/001 prepared by S.G.I. (2004), that had to be deconvoluted at the bedrock depth at then re-propagated through each foundation soil deposit.

These analysis provided the average strain levels within the soil interacting with each foundation, and allowed to select relevant values of the shear stiffness and damping ratio to be used in the evaluation of the stiffness and damping matrices.

Dynamic stiffness and damping coefficients depend on the loading frequency. The predominant loading frequency for each contact point was related to the fundamental modes of the structural element, in cooperation with the bridge designers.

2 Introduction

This report summarises the results of a number of seismic response analyses carried out at the sites of the tower foundations and the anchor blocks of the Messina bridge. The seismic response analyses were performed in free-field one-dimensional conditions, in order to estimate equivalent values of the soil stiffness and damping that are mobilised during the design earthquake. Results this analysis were used to evaluate the dynamic impedance matrices at each of the contact points of the structural model with the ground.

3 Input Motion

The reference seismic input used in this study included the acceleration time-hystories presented in Document DT/ISP/S/E/R1/001 prepared by S.G.I. (2004). This document contains two different batches of synthetic acceleration time histories the Sicily and the Calabria shores, each composed by 20 records. This seismic input was generated using a mathematical model of the seismogenetic source, and subsequently propagated to the soil surface at the Sicilian and Calabrian ground surface using a linear visco-elastic soil model. It should be noted that soil non-linearity was not considered when generating this seismic input.

For the present analysis, the horizontal NS and EW components of the accelerograms were composed in the longitudinal direction of the bridge and were subsequently deconvoluted to a specific depth that represents the bedrock for the subsequent propagation analyses. Deconvolution was carried out assuming essentially the same soil properties adopted by the authors of Document DT/ISP/S/E/R1/001, and specifically a linear visco-elastic soil behaviour. The parameters used in the analysis are reported in Tables 1 to 4: they are consistent with those used for propagating the signals in the coastal deposits, as reported in Document DT/ISP/S/E/R1/001.

It should be noted that in the propagation analysis damping is frequency-dependent, and is expressed in terms of the quality factor $Q = 1/(2D)$ as:

$Q = Q_0 f$

while in the deconvolution a constant damping coefficient $D = 2.5\ \%$ was used, corresponding, for $Q_0 = 20$ s, to a frequency of 1 Hz. For deposits with Vs > 800 m/s, a smaller damping ratio was selected, equal to 1 %.

Table 1 – Soil parameters used for deconvolution at the Sicily tower location.

Thickness (m)	V_S (m/s)	D (%)
62.5	200	2.5
21.5	300	2.5

Table 2 – Soil parameters used for deconvolution at the Sicily anchor block location.

Thickness (m)	V_S (m/s)	D (%)
62.5	200	2.5
21.5	300	2.5
12.5	1000	1.0

Table 3 – Soil parameters used for deconvolution at the Calabria tower location.

Thickness (m)	V_S (m/s)	D (%)
12.5	200	2.5
25.0	300	2.5
75.5	650	2.5

Table 4 – Soil parameters used for deconvolution at the Calabria anchor block location.

Thickness (m)	V_S (m/s)	D (%)
12.5	200	2.5
25.0	300	2.5
75.5	650	2.5
50.0	1000	1.0
17.5	1700	1.0

Tables 5 and 6 summarise the main characteristics of the deconvoluted accelerograms. In these tables a_{max} is the peak acceleration; T_m the mean period as defined by Rathje et al (1997); D_s is the significant duration (between 5 % and 95 % of I_A); and I_A is the Arias intensity.

Table 5 - Properties of Sicily bedrock accelerograms.

	Tower					Anchor Block				
No.	a_{max} (g)	T_m (s)	T_P (s)	D_B (s)	I_A (m/s)	a_{max} (g)	T_m (s)	T_P (s)	D_B (s)	I_A (m/s)
1	0.078	0.93	0.18	11.09	0.098	0.070	1.03	0.18	11.12	0.085
2	0.096	1.17	0.20	11.48	0.162	0.087	1.25	0.28	11.47	0.147
3	0.084	0.64	0.16	12.36	0.107	0.076	0.73	0.26	12.51	0.090
4	0.209	0.37	0.20	12.12	0.543	0.159	0.43	0.20	12.25	0.437
5	0.097	0.83	0.20	12.03	0.165	0.087	0.91	0.20	12.23	0.145
6	0.077	1.03	0.20	10.39	0.099	0.069	1.11	0.20	10.27	0.090
7	0.063	1.40	0.20	9.82	0.072	0.058	1.49	0.20	9.68	0.067
8	0.087	1.03	0.20	10.94	0.132	0.087	1.16	0.20	10.85	0.116
9	0.070	1.24	0.28	11.18	0.095	0.064	1.33	0.28	11.23	0.086
10	0.104	0.78	0.20	12.00	0.193	0.097	0.87	0.20	12.04	0.164
11	0.121	0.60	0.16	12.06	0.184	0.108	0.67	0.16	12.15	0.156
12	0.076	0.82	0.20	10.99	0.068	0.075	0.91	0.20	10.76	0.062
13	0.093	0.76	0.14	12.15	0.180	0.084	0.85	0.16	12.18	0.154
14	0.117	0.61	0.18	11.37	0.194	0.107	0.70	0.18	11.39	0.162
15	0.104	0.99	0.20	11.27	0.144	0.096	1.07	0.20	11.21	0.130
16	0.076	0.73	0.16	12.72	0.098	0.069	0.82	0.16	12.97	0.085
17	0.164	0.53	0.15	12.69	0.305	0.140	0.60	0.16	12.78	0.253
18	0.083	1.28	0.20	9.24	0.094	0.072	1.39	0.20	8.61	0.085
19	0.043	0.89	0.12	12.21	0.033	0.039	1.00	0.20	12.32	0.029
20	0.073	0.99	0.58	10.89	0.104	0.062	1.10	0.58	10.84	0.091

Table 6 - Properties of Calabria bedrock accelerograms.

	Tower					Anchor Block				
No.	a_{max} (g)	T_m (s)	T_P (s)	D_B (s)	I_a (m/s)	a_{max} (g)	T_m (s)	T_P (s)	D_B (s)	I_a (m/s)
1	0.127	0.66	0.24	11.25	0.275	0.105	0.76	0.30	10.26	0.179
2	0.117	0.81	0.42	11.11	0.242	0.098	0.98	0.56	10.77	0.142
3	0.136	0.64	0.24	12.12	0.300	0.096	0.76	0.12	12.17	0.181
4	0.208	0.68	0.06	11.29	0.464	0.143	0.76	0.06	11.71	0.247
5	0.097	0.59	0.18	12.17	0.162	0.082	0.65	0.32	13.00	0.115
6	0.129	0.66	0.16	11.38	0.224	0.104	0.84	0.16	11.13	0.116
7	0.080	0.86	0.24	11.17	0.136	0.076	1.00	0.36	11.65	0.088
8	0.125	0.86	0.40	12.00	0.213	0.122	0.96	0.62	12.49	0.133
9	0.142	0.67	0.10	11.81	0.277	0.121	0.74	0.62	11.39	0.196
10	0.144	0.86	0.24	11.91	0.318	0.124	0.93	0.30	12.20	0.214
11	0.063	0.59	0.22	11.95	0.062	0.049	0.70	0.54	12.17	0.037
12	0.126	0.53	0.22	11.64	0.229	0.105	0.64	0.16	11.64	0.131
13	0.101	0.83	0.16	11.29	0.194	0.106	0.92	0.16	11.37	0.125
14	0.115	0.63	0.18	11.57	0.209	0.084	0.72	0.18	11.88	0.109
15	0.140	0.95	0.16	10.21	0.172	0.105	1.11	0.50	9.39	0.107
16	0.086	1.26	0.16	10.20	0.143	0.071	1.41	0.12	10.56	0.099
17	0.156	0.90	0.10	10.75	0.269	0.116	0.98	0.32	10.59	0.183
18	0.158	0.79	0.10	11.05	0.269	0.120	0.95	0.10	11.41	0.161
19	0.100	0.61	0.16	11.92	0.097	0.090	0.72	0.16	11.22	0.071
20	0.130	0.71	0.50	11.62	0.218	0.096	0.80	0.34	11.92	0.140

4 Seismic Response Analysis

4.1 Methodology

One-dimensional site response analyses were performed with the visco-elastic non-linear equivalent model, using the code EERA (Bardet et al 2000). A total of 80 analyses were performed, one for each acceleration time history at the four locations of the foundation elements.

The soil deposit was subdivided in small layers, and each soil layer was assigned the properties of a non-linear viscoelastic material, that is, the small-strain shear modulus G_0, a modulus decay curve, and a damping curve that describes the increment of the equivalent damping D with shear strain.

The deconvoluted acceleration time histories were applied directly at a bedrock located at the same bedrock depth assumed in the deconvolution analysis (option “inside” or “within”).The effect of the bedrock deformability at larger depths was implicitly taken into account by the procedure used to obtain the seismic input.

4.2 Soil profile and mechanical properties

The small-strain shear modulus was evaluated directly from the results of cross-hole tests, carried out at each location of the foundation elements during the preliminary design stage. Figure 1 shows the distribution with depth of the small strain shear modulus G_0, evaluated assuming a soil density $\rho = 2$ Mg/m^3, together with the step-wise approximation used in the site response analyses.

Experimental observation of the modulus decay and damping curves are not available at the present stage. Therefore, the present study uses curves taken from the scientific literature to describe the variation of the secant shear stiffness G and damping ratio D with shear strain. Figure 2 shows the modulus decay and damping curves assumed for the coastal gravel deposits and the transition layers (Fig. 2a) and for the underlying stiff gravel deposit and/or Pezzo Conglomerate (Fig. 2b). The former derive from data published by Tanaka *et al*. (1987), while the latter, relative to rock or rock-like soils, are due to Idriss (1990).

4.3 Results of the propagation analysis

Figure 3 shows the profiles of the maximum acceleration computed in the site response analysis for each of the four locations analysed. For both the Sicily and Calabria sides,

the largest accelerations are produced by the acceleration time history No.4, that has Arias Intensity and peak accelerations significantly larger than the remaining input records (see also Tables 5 and 6). At the depth of each sub-layer centre, values of the equivalent secant shear modulus *G* and equivalent damping ratio *D* obtained from the different accelerograms were averaged, resulting in the profiles shown in Figures 4 to 7. Since the analytical solutions that were used to derive the dynamic impedance refer to foundations resting on a homogenous soil layer, *G* and *D* were in turn averaged over the soil depth directly interacting with the foundations, weighting the average according to the distribution of vertical stress induced by a rigid foundation on an elastic continuum. The average values of *G* and *D* obtained using this procedure are shown in Figures 4-7 with continuous lines and are summarised in Table 7.

Table 7 – Average values of *G* and *D* obtained from the site response analyses.

Site	*G* (MPa)	*D* (%)
Sicily Tower	110	8.3
Sicily Anchor Block	158	5.0
Calabria Tower	645	2.3
Calabria Anchor Block	1214	1.5

5 Dynamic Impedance of Tower Foundation

5.1 Background

Gazetas (1991) published a number of solutions for the evaluation of the dynamic impedance of foundations subjected to dynamic loads. In these solutions the subsoil is regarded as a linear visco-elastic medium.

For a given vibration mode, and for harmonic loads of circular frequency ω, the dynamic impedance $\mathcal{K}$ is defined as the ratio of the dynamic load $P(t)$ to the corresponding displacement $u(t)$. As the functions $P(t)$ and $u(t)$ are generally out of phase, the dynamic impedance $\mathcal{K}$ is complex-valued; this may be expressed as:

$$\mathcal{K}(\omega) = K_d(\omega) + i\,\omega\,C_d(\omega)$$

where *i* is the imaginary unit. Both K_d and C_d are functions of ω. The real part of $\mathcal{K}$, K_d, is termed *dynamic stiffness*, while C_d is a *dashpot coefficient*, which reflects both geometric and hysteretic damping.

While the solutions published by Gazetas (1991) refer strictly to a foundation subjected to an harmonic load, produced for instance by a vibratory machine, they can be used also for seismic loading if the inertial forces transmitted by the structure to the foundation can be approximated to a load varying harmonically with time.

To this purpose, it was assumed that the foundation elements transfer the seismic load to the foundations with a frequency derived from a modal analysis of the structural elements. Values of this frequency for the different foundation elements were derived from those provided by the designer (COWI A/S). For the Tower foundations and for the terminal structures, frequencies corresponding to longitudinal and transversal modes were averaged. For the anchor blocks, the frequency correspond to the inertial behaviour of the blocks, and are consistent with the secant shear moduli shown in Figs 5 and 7.

The dynamic impedance was evaluated for the tower foundations, for the anchor blocks, and for the foundations of the terminal structures. For these latter structures, located in the vicinity of the towers, the same soil profile and mechanical properties used for the analysis of the tower foundations were used.

Table 8 – Loading frequency *f* for the Tower foundations, the anchor blocks, and the terminal structures.

	f (Hz)
Sicily Tower	0.4
Sicily Anchor Block	2.0
Sicily Terminal Structure	1.8
Calabria Tower	0.4
Calabria Anchor Block	5.5
Calabria Terminal Structure	7.7

5.2 Evaluation of dynamic impedance

In the solutions published by Gazetas (1991), the dynamic stiffness K_d is obtained for each of the six vibration modes (three translations and three rotations) as:

$K_d = K \cdot k(\omega)$

where K is the static stiffness and $k(\omega)$ is a dynamic stiffness coefficient. The dashpot coefficient C_d is evaluated as:

$C_d = C_r + C_h = C_r + 2\, K_d\, D / \omega$

where C_r is the dashpot coefficient associated to radiation damping and $C_h = 2\, K_d\, D / \omega$ is the dashpot coefficient associated to hysteretic damping.

The analysis uses a frame of reference (x, y, z) in which the z axis is vertical and oriented downwards; the y axis is horizontal, parallel to the longitudinal direction of the bridge and oriented southward (from Sicily to Calabria); the *x* axis is horizontal and is oriented eastward. Rotations and moments are denoted by the rotation axis; note that clockwise rotations and moments around the *x* axis (*rx)* are positive (see Fig. 8).

The stiffness and damping matrices was first evaluated at the bottom of the equivalent foundation, along its centre-line (points denoted A), and then was transformed to provide the force-displacement relationship for the reference points (denoted G) located by the structural analyst (Cowi A/C).

Figure 9 shows a layout of an embedded rectangular foundation, with symbols used to denote the geometry. Figures 10 and 11 show the idealised foundations for the Sicily and the Calabria towers. The equivalent foundation includes the circular footings and the volume of soil treated with jet-grouting below the footing, while it neglects the lateral soil treated with a sparser jet-grouting. In Figs 10 and 11, open circles indicate points (A) where the impedance matrix was originally evaluated, while full circles designate points (G), that is, the position of the elastic elements that represent the soil-foundation stiffness. These reference points correspond with the intersection of the tower axes with the bottom of the circular footings.

Figures 12 and 13 display the schemes used for the anchor blocks: they were regarded as rectangular foundations embedded in an elastic layer. For the anchor blocks, the reference point (G) is the centre of gravity.

Figure 14 and 15 show the idealised foundations of the terminal structures on the Sicily and the Calabria shores. Each viaduct has two independent foundations that were given two identical impedance matrixes. The impedance matrix of each of these foundations has a structure similar to that of the tower foundations.

For all the foundation elements, coupling occurs between the rotations *rx*, *ry* and the horizontal forces along *x* and *y* (and, equivalently, between the displacements along *x* and y and the moments *ry* and *rx*). These coupled terms are indicated with subscripts y-rx and x-ry.

Details of the calculations are reported in Appendix A, while the complete set of solutions obtained by Gazetas (1991) are reproduced in the Appendix B.

5.3 Verification of the elastic solutions

An independent check of the validity of the elastic solutions provided by Gazetas (1991) was carried out with specific reference to the vertical displacement of one of the embedded foundations of the Sicily Tower. To this purpose, finite element numerical analyses were carried out with the code Plaxis v.8, in which a cylindrical foundation is loaded by a uniform vertical pressure that is an harmonic function of time with an amplitude of 100 kPa.

The axi-symmetric Plaxis finite element mesh used in the calculations is shown in Figure 16. The foundation soil is a homogenous visco-elastic layer with G = 110 MPa end ν = 0.2 and a damping ratio D = 5 %, resting on an infinitely rigid boundary which acts as a perfectly reflecting surface. The lateral sides of the mesh have absorbing boundaries of the type developed by Lysmer and Kuhlemeyer (1969). The analyses used a Newmark time-integration scheme with Newmark parameters equal to 0.25 and 0.5, in order not to generate any numerical damping.

The analyses were repeated for two different loading frequencies f_L, equal to 0.4 and 1.0 Hz. The Rayleigh damping parameters in the analysis was calibrated in order to produce a damping ratio of 5 % for $f = f_L$. The resulting Rayleigh α and β parameters are listed in Table 9.

Figure 17 shows a comparison between the results obtained from the numerical analyses and those predicted by Gazetas (1991) using the same elastic and damping properties: the cyclic relationship between the resultant vertical force on the foundation F_z and the corresponding vertical displacement w obtained using the two methods are

in a reasonable agreement, validating the use of the approximate Gazetas (1991) equations; these equations were then used to obtain the results presented in the following sections.

Table 9 . Rayleigh damping parameters

f_L (Hz)	α	β
0.4	0.105	0.327
1.0	0.024	0.008

6 Stiffness and Damping Matrices

Table 10 reports the matrices of the dynamic stiffness for the reference points provided by the structural analysts for the tower foundations, the anchor blocks, and the foundations of the terminal viaducts. The corresponding matrices of damping coefficients are reported in Table 11 units are kN and m.

6.1 Confidence intervals

Lower bound values for the dynamic impedances can be obtained using the small-strain shear stiffness and damping ratio. Conversely, the stiffness parameters obtained from the back-analysis of static three-dimensional finite element analysis (see Report CG1003-P-CL-D-P-CG-S4-00-00-00-00-01_A Equivalent Stiffness matrices for the Soil-Foundation System) are deemed a reasonable estimate of the lower bound stiffness coefficients. From these static stiffness coefficients, a corresponding damping ratio can be readily evaluated from the stiffness decay curves and the damping ratio increase curves of Figure 2, corresponding to the appropriate strain levels. Table 12 summarises the values of the equivalent elastic stiffness obtained for these upper and lower bounds. Using the values reported in Table 12, the stiffness and damping matrices were recalculated: they are reported in Tables 13 to 16.

Table 10. Dynamic stiffness matrices

Sicily Tower

	x	y	z	rx	ry	rz
x	5.5E+07	0	0	0	-5.7E+08	0
y	0	5.5E+07	0	-5.7E+08	0	0
z	0	0	5.3E+07	0	0	0
rx	0	-5.7E+08	0	3.3E+10	0	0
ry	-5.7E+08	0	0	0	3.3E+10	0
rz	0	0	0	0	0	5.5E+10

Units

x x	kN/m
y y	kN/m
z z	kN/m
rx rx	kN m
ry ry	kN m
rz rz	kN m
x ry	kN
y rx	kN

Calabria Tower

	x	y	z	rx	ry	rz
x	2.7E+08	0	0	0	-1.0E+09	0
y	0	2.7E+08	0	-1.0E+09	0	0
z	0	0	1.3E+08	0	0	0
rx	0	-1.0E+09	0	1.1E+11	0	0
ry	-1.0E+09	0	0	0	1.1E+11	0
rz	0	0	0	0	0	2.2E+11

Sicily Anchor

	x	y	z	rx	ry	rz
x	7.8E+07	0	0	0	8.7E+08	0
y	0	8.0E+07	0	8.9E+08	0	0
z	0	0	1.0E+08	0	0	0
rx	0	8.9E+08	0	9.8E+10	0	0
ry	8.7E+08	0	0	0	1.4E+11	0
rz	0	0	0	0	0	3.6E+11

Calabria Anchor

	x	y	z	rx	ry	rz
x	4.9E+08	0	0	0	3.3E+09	0
y	0	4.9E+08	0	3.3E+09	0	0
z	0	0	5.7E+08	0	0	0
rx	0	3.3E+09	0	6.9E+11	0	0
ry	3.3E+09	0	0	0	9.9E+11	0
rz	0	0	0	0	0	2.8E+12

Sicily terminal structure

	x	y	z	rx	ry	rz
x	2.3E+07	0	0	0	-7.7E+07	0
y	0	2.4E+07	0	-8.1E+07	0	0
z	0	0	1.8E+07	0	0	0
rx	0	-8.1E+07	0	1.5E+11	0	0
ry	-7.7E+07	0	0	0	1.9E+11	0
rz	0	0	0	0	0	2.7E+11

Calabria terminal structure

	x	y	z	rx	ry	rz
x	8.5E+07	0	0	0	3.6E+08	0
y	0	9.1E+07	0	3.9E+08	0	0
z	0	0	1.0E+08	0	0	0
rx	0	3.9E+08	0	4.8E+11	0	0
ry	3.6E+08	0	0	0	6.1E+11	0
rz	0	0	0	0	0	1.0E+12

\

Table 11. Damping matrices

Sicily Tower

	x	y	z	rx	ry	rz
x	4.1E+06	0	0	0	-4.3E+07	0
y	0	4.1E+06	0	-4.3E+07	0	0
z	0	0	4.0E+06	0	0	0
rx	0	-4.3E+07	0	2.5E+09	0	0
ry	-4.3E+07	0	0	0	2.5E+09	0
rz	0	0	0	0	0	4.1E+09

Calabria Tower

	x	y	z	rx	ry	rz
x	5.5E+06	0	0	0	-2.1E+07	0
y	0	5.5E+06	0	-2.1E+07	0	0
z	0	0	2.8E+06	0	0	0
rx	0	-2.1E+07	0	2.3E+09	0	0
ry	-2.1E+07	0	0	0	2.3E+09	0
rz	0	0	0	0	0	4.6E+09

Sicily Anchor

	x	y	z	rx	ry	rz
x	6.5E+05	0	0	0	7.0E+06	0
y	0	6.6E+05	0	7.2E+06	0	0
z	0	0	8.3E+05	0	0	0
rx	0	7.2E+06	0	2.7E+10	0	0
ry	7.0E+06	0	0	0	4.3E+10	0
rz	0	0	0	0	0	2.9E+09

Calabria Anchor

	x	y	z	rx	ry	rz
x	4.9E+05	0	0	0	2.7E+06	0
y	0	4.9E+05	0	2.7E+06	0	0
z	0	0	5.3E+05	0	0	0
rx	0	2.7E+06	0	5.6E+10	0	0
ry	2.7E+06	0	0	0	6.4E+10	0
rz	0	0	0	0	0	2.5E+09

Sicily terminal structure

	x	y	z	rx	ry	rz
x	2.2E+06	0	0	0	-1.4E+07	0
y	0	2.2E+06	0	-1.4E+07	0	0
z	0	0	3.0E+05	0	0	0
rx	0	-1.4E+07	0	2.3E+09	0	0
ry	-1.4E+07	0	0	0	3.0E+09	0
rz	0	0	0	0	0	4.4E+09

Calabria terminal structure

	x	y	z	rx	ry	rz
x	8.3E+05	0	0	0	2.6E+06	0
y	0	8.3E+05	0	2.6E+06	0	0
z	0	0	9.7E+04	0	0	0
rx	0	2.6E+06	0	4.3E+08	0	0
ry	2.6E+06	0	0	0	5.6E+08	0
rz	0	0	0	0	0	9.5E+08

Units	
x x	Mg/s
y y	Mg/s
z z	Mg/s
rx rx	Mg m^2 /s
ry ry	Mg m^2 /s
rz rz	Mg m^2 /s
x ry	Mg m /s
y rx	Mg m /s

Table 12 – Upper and lower bounds for *G* and *D*.

	Upper bound		Lower bound	
Site	*G* (MPa)	*D* (%)	*G* (MPa)	*D* (%)
Sicily Tower	200	2.5	60	12
Sicily Anchor Block	300	1.0	120	9
Calabria Tower	800	2.0	300	10
Calabria Anchor Block	1300	1.0	650	5

Table 13. Dynamic stiffness matrices - Upper bound

Sicily Tower

	x	y	z	rx	ry	rz
x	**1.0E+08**	0	0	0	**-1.0E+09**	0
y	0	**1.0E+08**	0	**-1.0E+09**	0	0
z	0	0	**9.7E+07**	0	0	0
rx	0	**-1.0E+09**	0	**6.2E+10**	0	0
ry	**-1.0E+09**	0	0	0	**6.2E+10**	0
rz	0	0	0	0	0	**1.0E+11**

Units

x x	kN/m
y y	kN/m
z z	kN/m
rx rx	kN m
ry ry	kN m
rz rz	kN m
x ry	kN
y rx	kN

Calabria Tower

	x	y	z	rx	ry	rz
x	**3.3E+08**	0	0	0	**-1.3E+09**	0
y	0	**3.3E+08**	0	**-1.3E+09**	0	0
z	0	0	**1.6E+08**	0	0	0
rx	0	**-1.3E+09**	0	**1.4E+11**	0	0
ry	**-1.3E+09**	0	0	0	**1.4E+11**	0
rz	0	0	0	0	0	**2.8E+11**

Sicily Anchor

	x	y	z	rx	ry	rz
x	**1.5E+08**	0	0	0	**1.7E+09**	0
y	0	**1.5E+08**	0	**1.7E+09**	0	0
z	0	0	**1.7E+08**	0	0	0
rx	0	**1.7E+09**	0	**2.4E+11**	0	0
ry	**1.7E+09**	0	0	0	**3.4E+11**	0
rz	0	0	0	0	0	**7.6E+11**

Calabria Anchor

	x	y	z	rx	ry	rz
x	**5.2E+08**	0	0	0	**3.5E+09**	0
y	0	**5.3E+08**	0	**3.5E+09**	0	0
z	0	0	**6.0E+08**	0	0	0
rx	0	**3.5E+09**	0	**7.7E+11**	0	0
ry	**3.5E+09**	0	0	0	**1.1E+12**	0
rz	0	0	0	0	0	**3.0E+12**

Sicily terminal structure

	x	y	z	rx	ry	rz
x	**4.1E+07**	0	0	0	**-1.4E+08**	0
y	0	**4.3E+07**	0	**-1.5E+08**	0	0
z	0	0	**3.2E+07**	0	0	0
rx	0	**-1.5E+08**	0	**2.7E+11**	0	0
ry	**-1.4E+08**	0	0	0	**3.5E+11**	0
rz	0	0	0	0	0	**5.0E+11**

Calabria terminal structure

	x	y	z	rx	ry	rz
x	**1.0E+08**	0	0	0	**4.5E+08**	0
y	0	**1.1E+08**	0	**4.8E+08**	0	0
z	0	0	**1.0E+08**	0	0	0
rx	0	**4.8E+08**	0	**7.8E+11**	0	0
ry	**4.5E+08**	0	0	0	**1.0E+12**	0
rz	0	0	0	0	0	**1.5E+12**

Table 14. Damping matrices - Upper bound

Sicily Tower

	x	y	z	rx	ry	rz
x	2.3E+06	0	0	0	-2.3E+07	0
y	0	2.3E+06	0	-2.3E+07	0	0
z	0	0	2.2E+06	0	0	0
rx	0	-2.3E+07	0	1.4E+09	0	0
ry	-2.3E+07	0	0	0	1.4E+09	0
rz	0	0	0	0	0	2.3E+09

Calabria Tower

	x	y	z	rx	ry	rz
x	1.5E+07	0	0	0	-5.8E+07	0
y	0	1.5E+07	0	-5.8E+07	0	0
z	0	0	7.4E+06	0	0	0
rx	0	-5.8E+07	0	6.3E+09	0	0
ry	-5.8E+07	0	0	0	6.3E+09	0
rz	0	0	0	0	0	1.2E+10

Sicily Anchor

	x	y	z	rx	ry	rz
x	2.7E+05	0	0	0	2.7E+06	0
y	0	2.8E+05	0	2.8E+06	0	0
z	0	0	2.9E+05	0	0	0
rx	0	2.8E+06	0	3.1E+10	0	0
ry	2.7E+06	0	0	0	5.0E+10	0
rz	0	0	0	0	0	1.3E+09

Calabria Anchor

	x	y	z	rx	ry	rz
x	3.7E+05	0	0	0	1.9E+06	0
y	0	3.7E+05	0	1.9E+06	0	0
z	0	0	3.9E+05	0	0	0
rx	0	1.9E+06	0	5.7E+10	0	0
ry	1.9E+06	0	0	0	6.5E+10	0
rz	0	0	0	0	0	1.8E+09

Sicily terminal structure

	x	y	z	rx	ry	rz
x	2.8E+06	0	0	0	-1.9E+07	0
y	0	2.8E+06	0	-1.9E+07	0	0
z	0	0	1.8E+05	0	0	0
rx	0	-1.9E+07	0	1.4E+09	0	0
ry	-1.9E+07	0	0	0	1.8E+09	0
rz	0	0	0	0	0	2.7E+09

Calabria terminal structure

	x	y	z	rx	ry	rz
x	2.0E+06	0	0	0	6.2E+06	0
y	0	2.0E+06	0	6.2E+06	0	0
z	0	0	8.8E+04	0	0	0
rx	0	6.2E+06	0	6.4E+08	0	0
ry	6.2E+06	0	0	0	8.3E+08	0
rz	0	0	0	0	0	1.3E+09

Units	
x x	Mg/s
y y	Mg/s
z z	Mg/s
rx rx	Mg m^2 /s
ry ry	Mg m^2 /s
rz rz	Mg m^2 /s
x ry	Mg m /s
y rx	Mg m /s

Table 15. Dynamic stiffness matrices - Lower bound

Sicily Tower

	x	y	z	rx	ry	rz
x	**3.0E+07**	0	0	0	**-3.1E+08**	0
y	0	**3.0E+07**	0	**-3.1E+08**	0	0
z	0	0	**2.9E+07**	0	0	0
rx	0	**-3.1E+08**	0	**1.8E+10**	0	0
ry	**-3.1E+08**	0	0	0	**1.8E+10**	0
rz	0	0	0	0	0	**3.0E+10**

Units

x x	kN/m
y y	kN/m
z z	kN/m
rx rx	kN m
ry ry	kN m
rz rz	kN m
x ry	kN
y rx	kN

Calabria Tower

	x	y	z	rx	ry	rz
x	**1.2E+08**	0	0	0	**-4.8E+08**	0
y	0	**1.2E+08**	0	**-4.8E+08**	0	0
z	0	0	**6.2E+07**	0	0	0
rx	0	**-4.8E+08**	0	**5.2E+10**	0	0
ry	**-4.8E+08**	0	0	0	**5.2E+10**	0
rz	0	0	0	0	0	**1.0E+11**

Sicily Anchor

	x	y	z	rx	ry	rz
x	**5.9E+07**	0	0	0	**6.6E+08**	0
y	0	**6.1E+07**	0	**6.8E+08**	0	0
z	0	0	**8.4E+07**	0	0	0
rx	0	**6.8E+08**	0	**6.3E+10**	0	0
ry	**6.6E+08**	0	0	0	**9.4E+10**	0
rz	0	0	0	0	0	**2.6E+11**

Calabria Anchor

	x	y	z	rx	ry	rz
x	**2.6E+08**	0	0	0	**1.8E+09**	0
y	0	**2.6E+08**	0	**1.8E+09**	0	0
z	0	0	**3.7E+08**	0	0	0
rx	0	**1.8E+09**	0	**2.2E+11**	0	0
ry	**1.8E+09**	0	0	0	**3.4E+11**	0
rz	0	0	0	0	0	**1.3E+12**

Sicily terminal structure

	x	y	z	rx	ry	rz
x	**1.4E+07**	0	0	0	**-4.7E+07**	0
y	0	**1.5E+07**	0	**-5.0E+07**	0	0
z	0	0	**1.1E+07**	0	0	0
rx	0	**-5.0E+07**	0	**8.8E+10**	0	0
ry	**-4.7E+07**	0	0	0	**1.1E+11**	0
rz	0	0	0	0	0	**1.6E+11**

Calabria terminal structure

	x	y	z	rx	ry	rz
x	**3.6E+07**	0	0	0	**1.5E+08**	0
y	0	**3.9E+07**	0	**1.7E+08**	0	0
z	0	0	**3.8E+07**	0	0	0
rx	0	**1.7E+08**	0	**2.4E+11**	0	0
ry	**1.5E+08**	0	0	0	**3.1E+11**	0
rz	0	0	0	0	0	**4.9E+11**

Table 16. Damping matrices - Lower bound

Sicily Tower

	x	y	z	rx	ry	rz
x	3.3E+06	0	0	0	-3.4E+07	0
y	0	3.3E+06	0	-3.4E+07	0	0
z	0	0	3.2E+06	0	0	0
rx	0	-3.4E+07	0	1.9E+09	0	0
ry	-3.4E+07	0	0	0	1.9E+09	0
rz	0	0	0	0	0	3.2E+09

Units

x x	Mg/s
y y	Mg/s
z z	Mg/s
rx rx	Mg m^2 /s
ry ry	Mg m^2 /s
rz rz	Mg m^2 /s
x ry	Mg m /s
y rx	Mg m /s

Calabria Tower

	x	y	z	rx	ry	rz
x	1.1E+07	0	0	0	-4.3E+07	0
y	0	1.1E+07	0	-4.3E+07	0	0
z	0	0	5.6E+06	0	0	0
rx	0	-4.3E+07	0	4.7E+09	0	0
ry	-4.3E+07	0	0	0	4.7E+09	0
rz	0	0	0	0	0	9.3E+09

Sicily Anchor

	x	y	z	rx	ry	rz
x	9.1E+05	0	0	0	1.0E+07	0
y	0	9.3E+05	0	1.0E+07	0	0
z	0	0	1.3E+06	0	0	0
rx	0	1.0E+07	0	2.5E+10	0	0
ry	1.0E+07	0	0	0	4.0E+10	0
rz	0	0	0	0	0	3.9E+09

Calabria Anchor

	x	y	z	rx	ry	rz
x	7.3E+05	0	0	0	4.5E+06	0
y	0	7.4E+05	0	4.5E+06	0	0
z	0	0	9.9E+05	0	0	0
rx	0	4.5E+06	0	4.6E+10	0	0
ry	4.5E+06	0	0	0	5.2E+10	0
rz	0	0	0	0	0	3.4E+09

Sicily terminal structure

	x	y	z	rx	ry	rz
x	1.8E+06	0	0	0	-1.2E+07	0
y	0	1.8E+06	0	-1.2E+07	0	0
z	0	0	2.7E+05	0	0	0
rx	0	-1.2E+07	0	2.0E+09	0	0
ry	-1.2E+07	0	0	0	2.6E+09	0
rz	0	0	0	0	0	3.8E+09

Calabria terminal structure

	x	y	z	rx	ry	rz
x	1.3E+06	0	0	0	4.0E+06	0
y	0	1.3E+06	0	4.1E+06	0	0
z	0	0	1.6E+05	0	0	0
rx	0	4.1E+06	0	9.8E+08	0	0
ry	4.0E+06	0	0	0	1.3E+09	0
rz	0	0	0	0	0	2.0E+09

References

Bardet J.P., Ichii K. & Lin C.H. (2000). EERA. *A computer program for equivalent linear earthquake site response analysis of layered soil deposits*. Dept. of Civil Engineering, University of southern California.

Gazetas G. (1991). Foundation vibrations. In: *Foundation Engineering Handbook, 2nd edition*, H.-Y. Fang, ed., Van Nostrand Reinhold, New York, 553-593.

Hudson M., Idriss I.M. & Beikae M. (1994). QUAD4M. A computer program to evaluate the seismic response of soil structures using finite element procedures and incorporating a compliant base. Center for Geotechnical Modeling, Dept. of Civil and Environmental Engineering, University of California, Davis.

Idriss I. M. (1990). Response of Soft Soil Sites during Earthquakes. *Proceedings, Memorial Symposium to honor Professor Harry Bolton Seed*, Berkeley, California, Vol. II.

Khran J. (2004). *Dynamic modelling with QUAKE/W*. GEO-SLOPE International Ltd.

Lysmer, J., and Kuhlemeyer R.L. (1969) Finite dynamic model for infinite media, Journal of Engineering Mechanics, Vol. 95(EM4), 859-877.

ProShake (1999) Edu Pro Civil Systems Inc.

Rathje E.M., Abrahamson N.A. & Bray J.D. (1998). Simplified frequency content estimates of earthquake ground motion. *Journal of Geotechncial and Geoenvironmental Engineering*, ASCE, Vol. 124, No.2: 150-159.

Tanaka Y., Kudo Y., Yoshida Y. & Ikemi M. (1987). *A study on the mechanical properties of sandy gravel – dynamic properties of reconstituted samples*. Central Research Institute of Electric Power Industry, Report U87019.

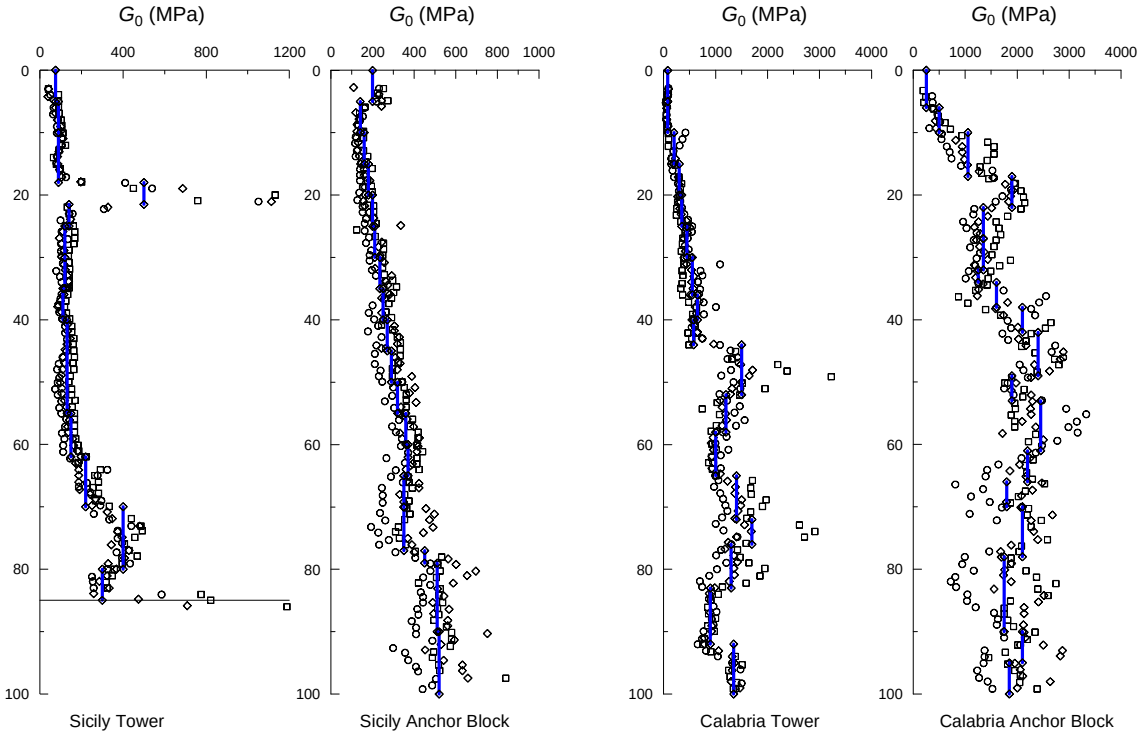

Figure 1. Profiles of the small strain stiffness obtained from cross-hole tests and adopted in the analysis.

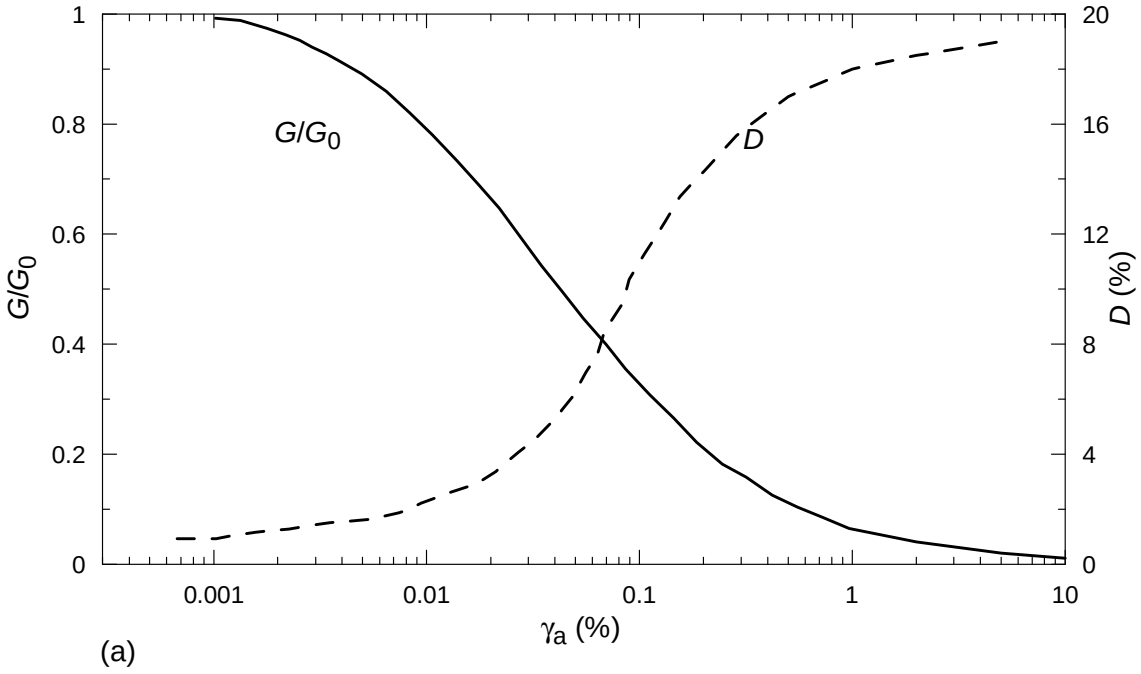

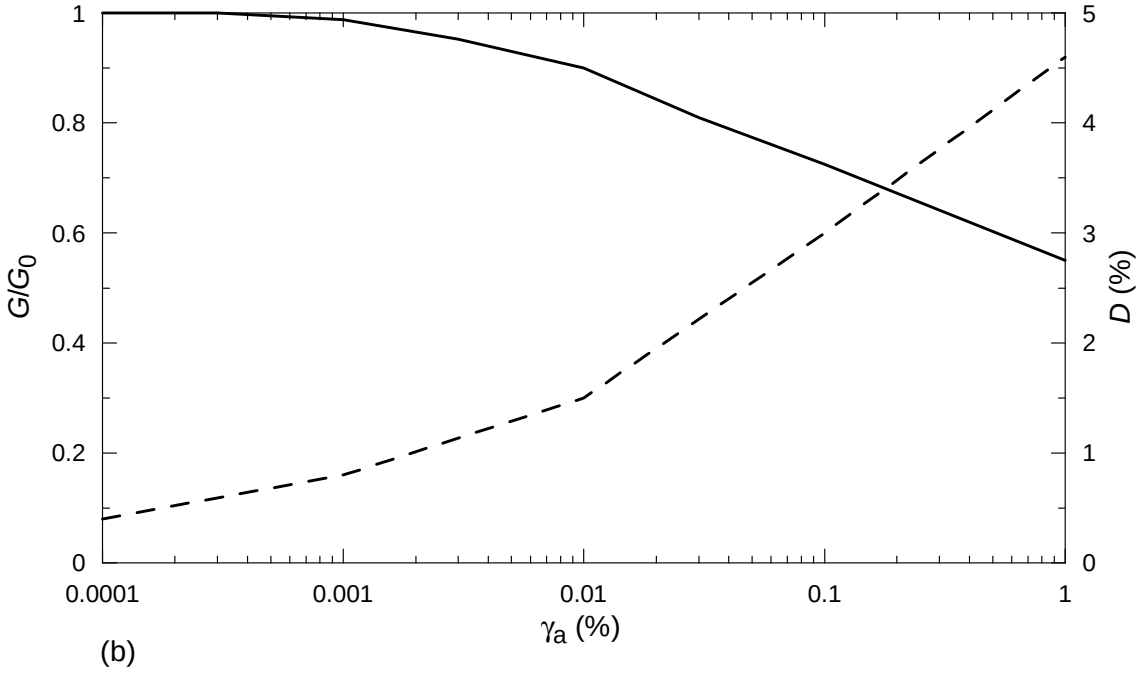

Figure 2 - Modulus decay and damping curves used in the site response analysis at the Sicily Tower location: a) coastal deposits; b) (bedrock).

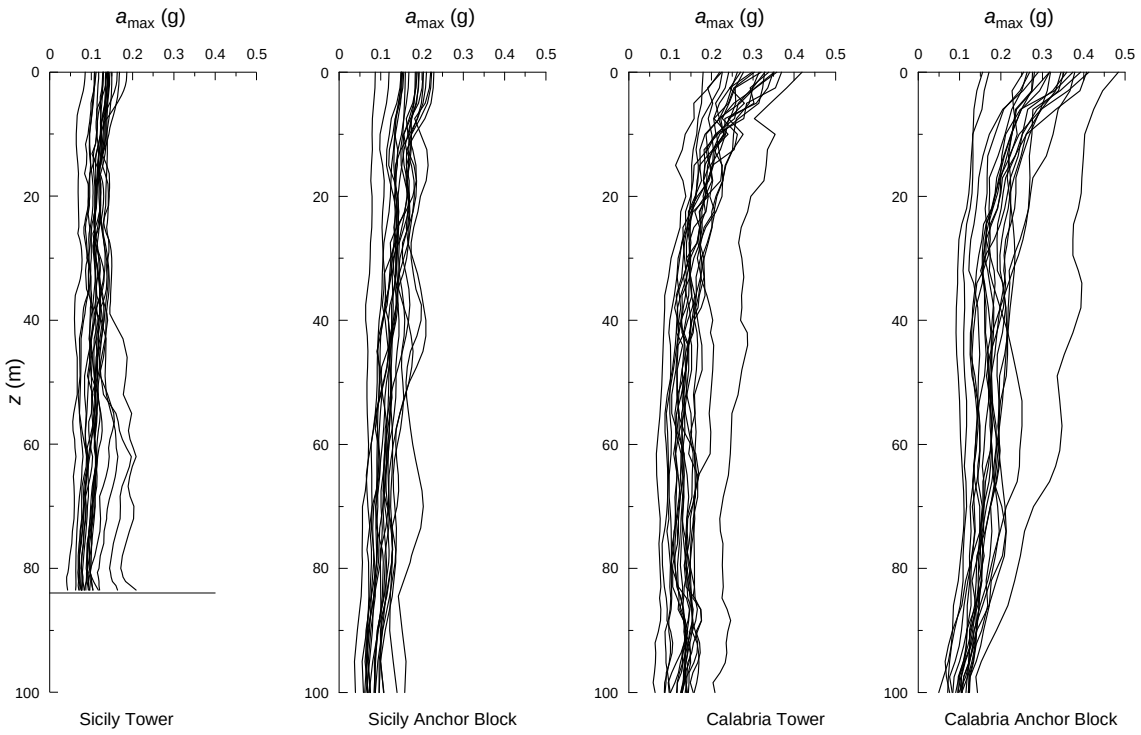

Figure 3. Profiles of the maximum acceleration computed in the site response analyses.

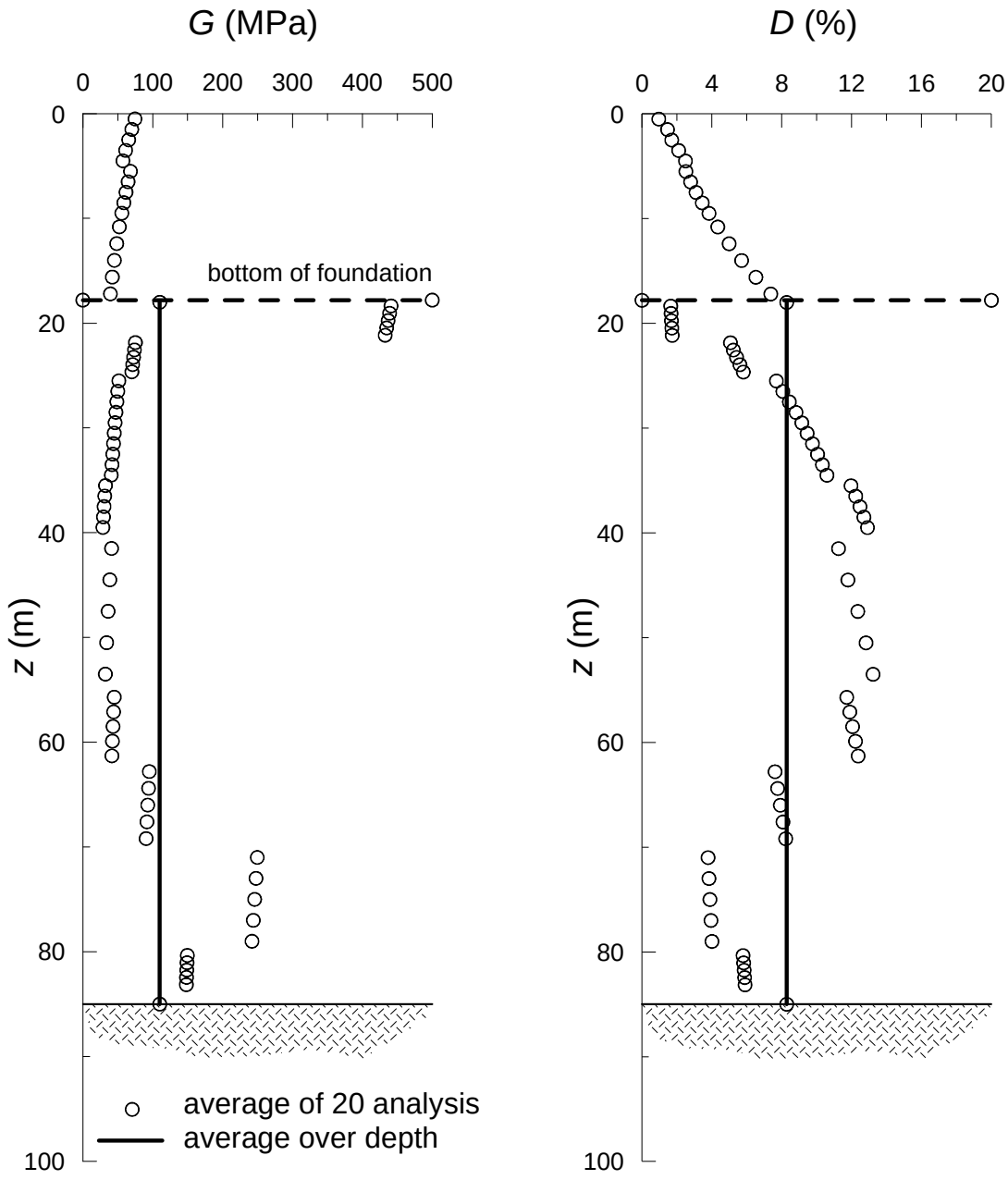

Figure 4. Average values of secant stiffness G and damping ratio D for the Sicily Tower.

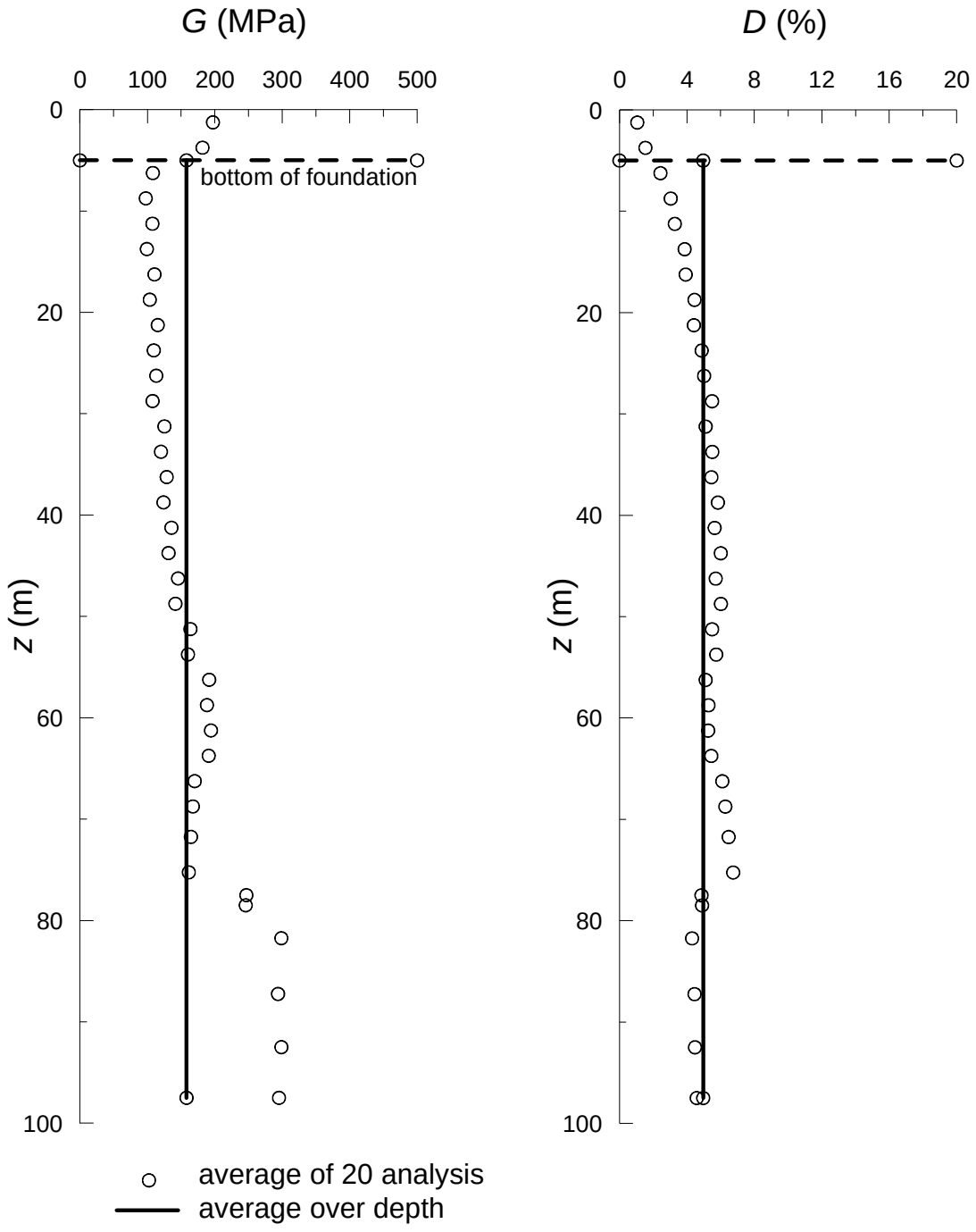

Figure 5. Average values of secant stiffness G and damping ratio D for the Sicily Anchor Block.

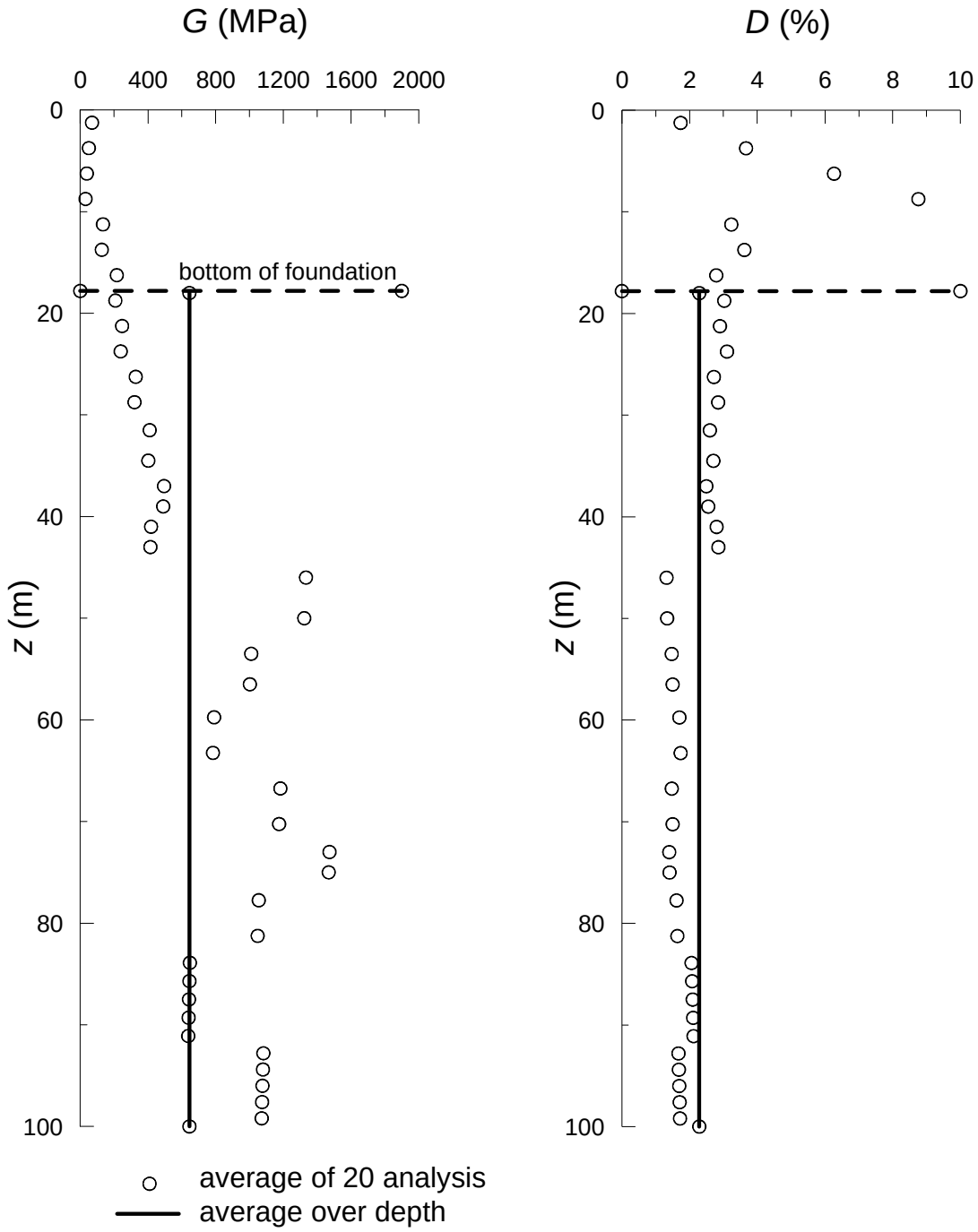

Figure 6. Average values of secant stiffness G and damping ratio D for the Calabria Tower.

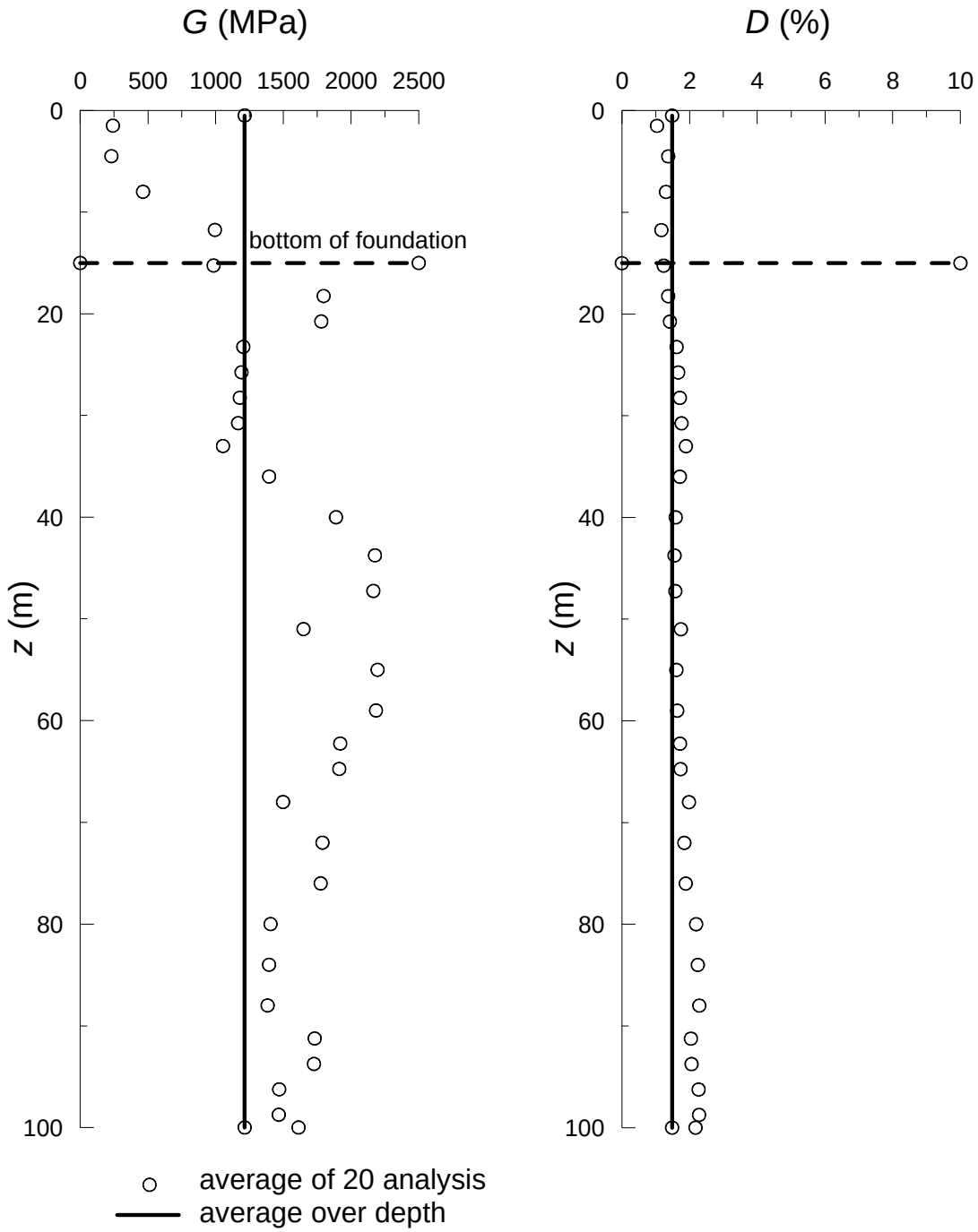

Figure 7. Average values of secant stiffness G and damping ratio D for the Calabria Anchor Block.

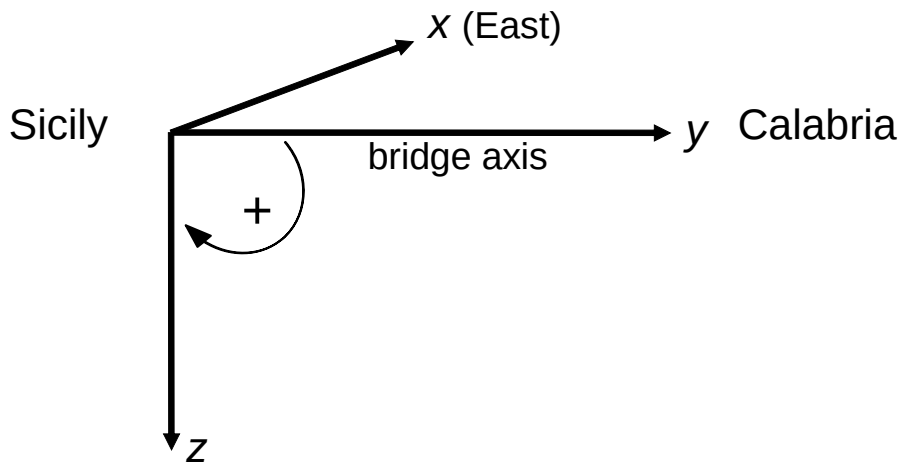

Figure 8. Frame of reference used in the calculations.

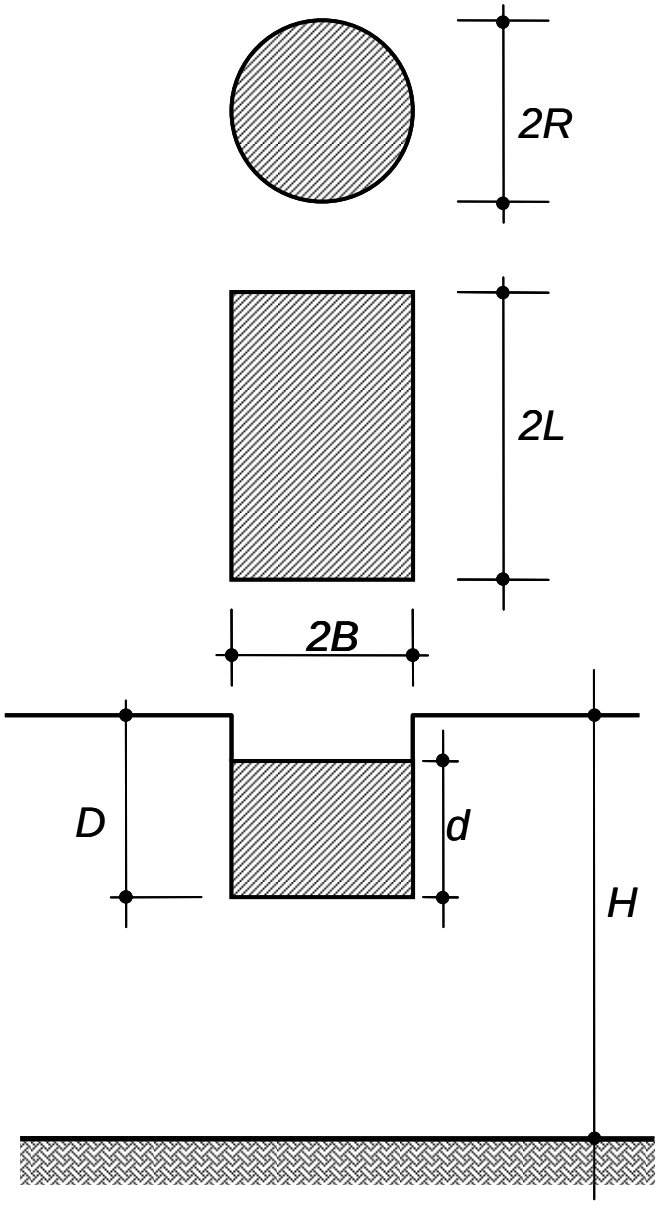

Figure 9. Schematic layout of an embedded rectangular foundation embedded in and elastic half-space.

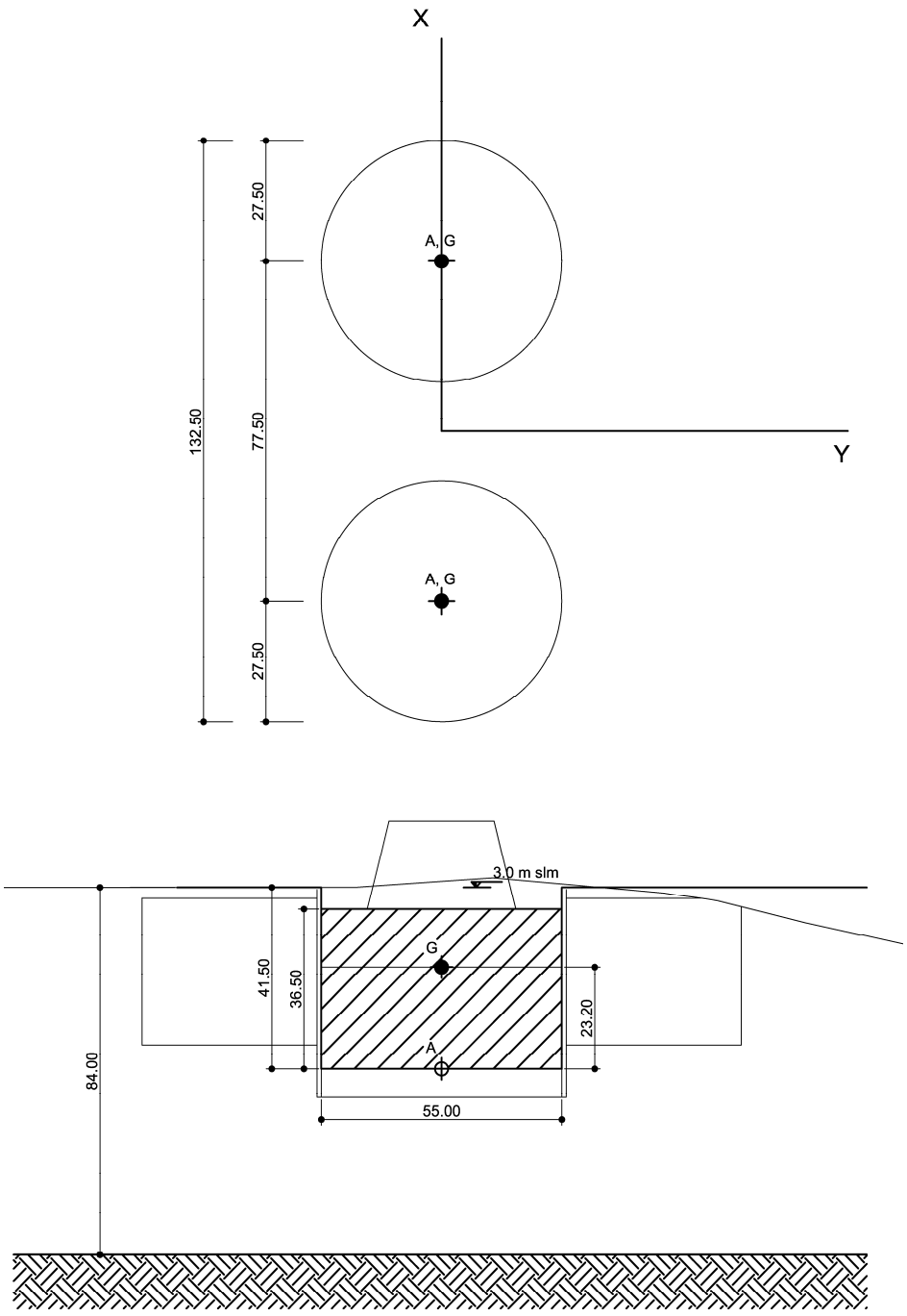

Figure 10. Foundation of the Sicily Tower.

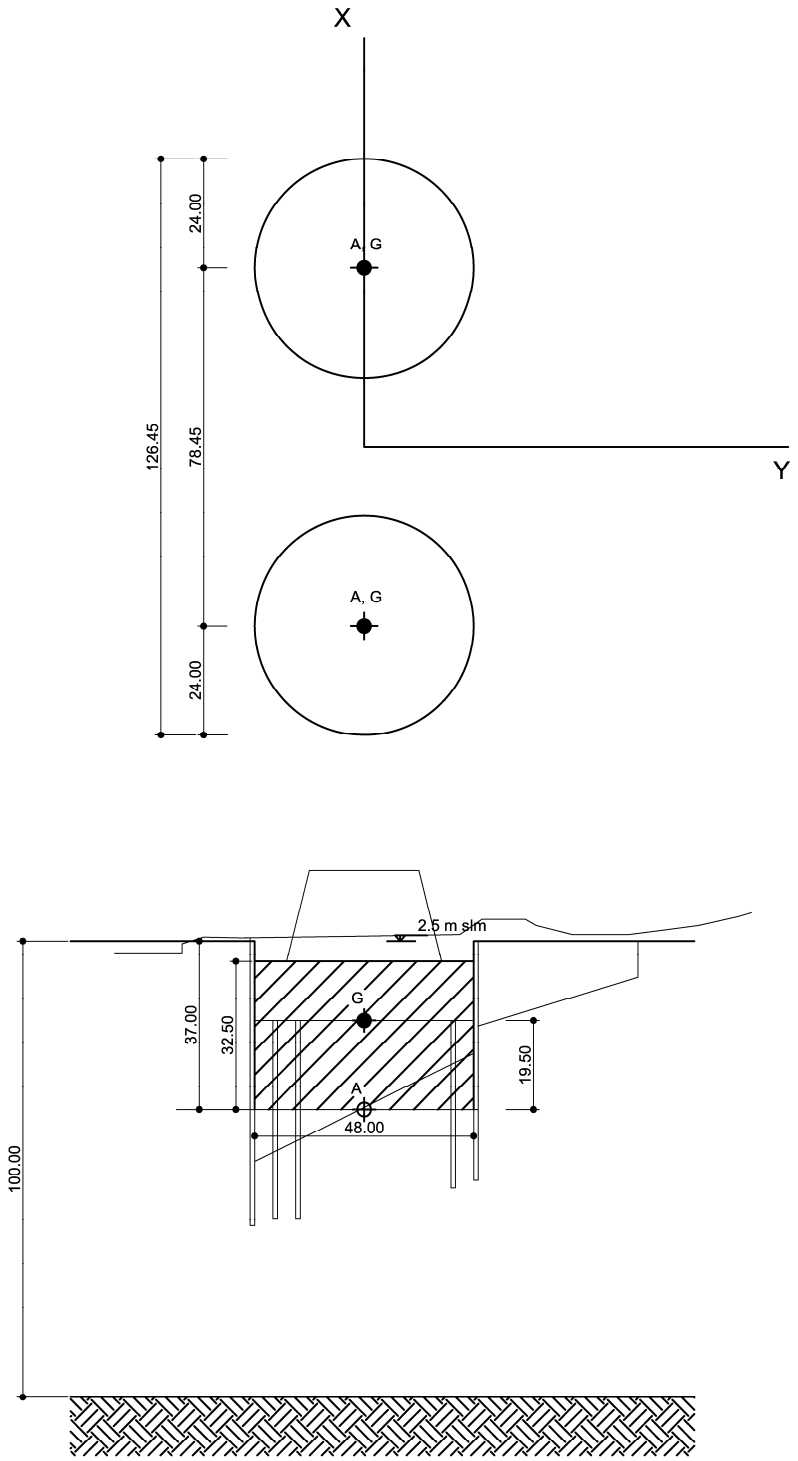

Figure 11. Foundation of the Calabria Tower.

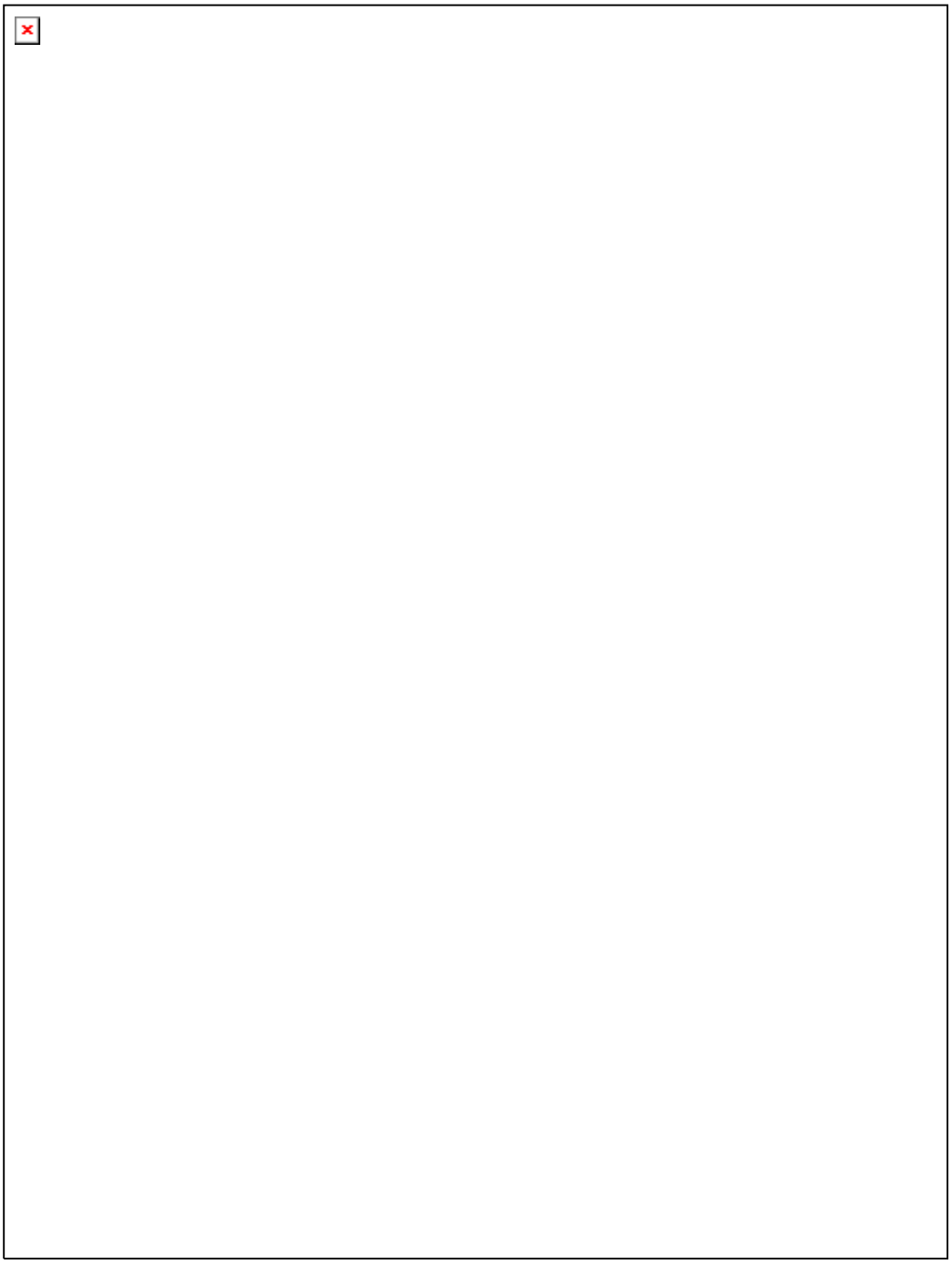

Figure 12. Foundation of the Sicily anchor block.

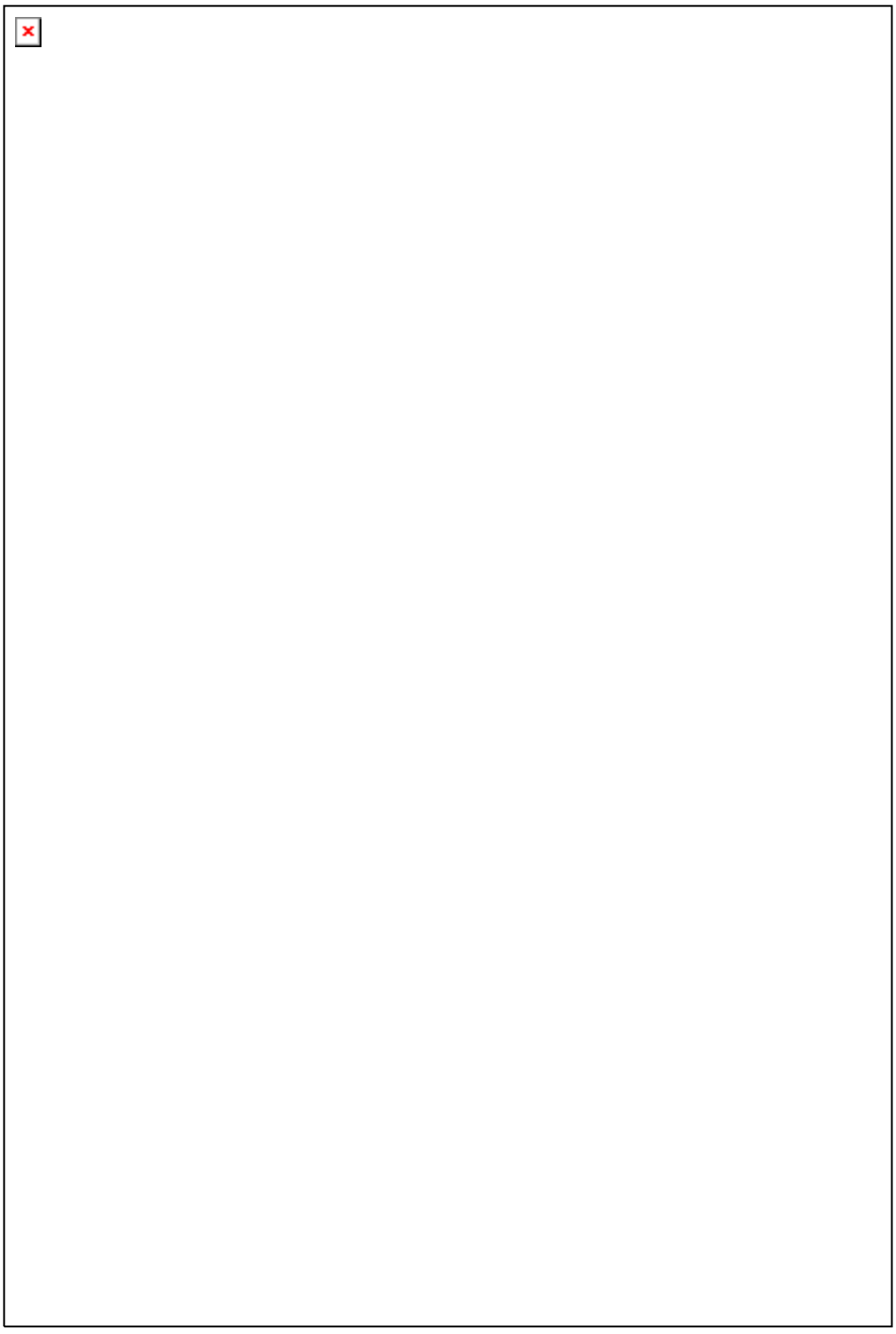

Figure 13. Foundation of the Calabria anchor block.

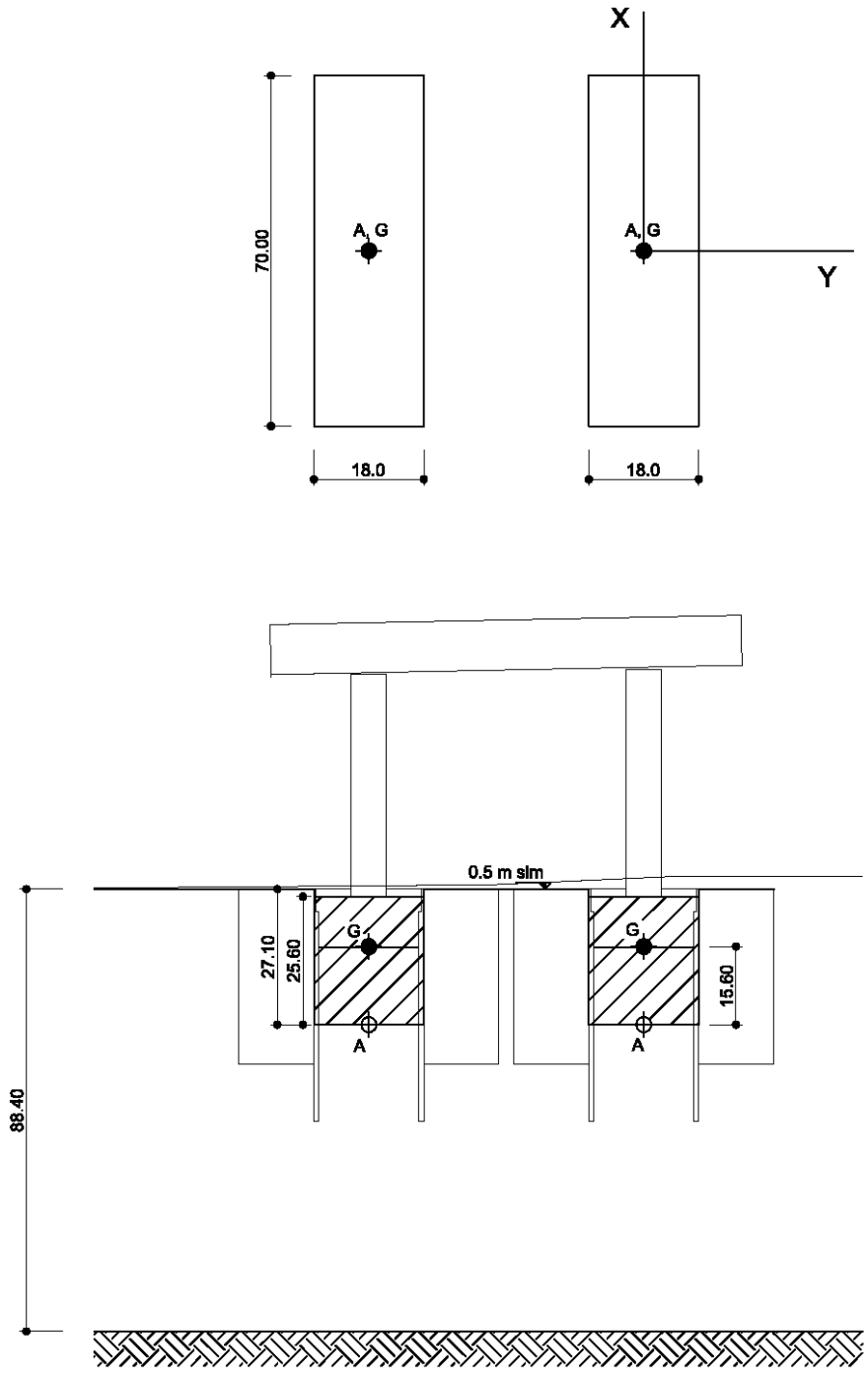

Figure 14. Foundations of the Sicilia terminal structure.

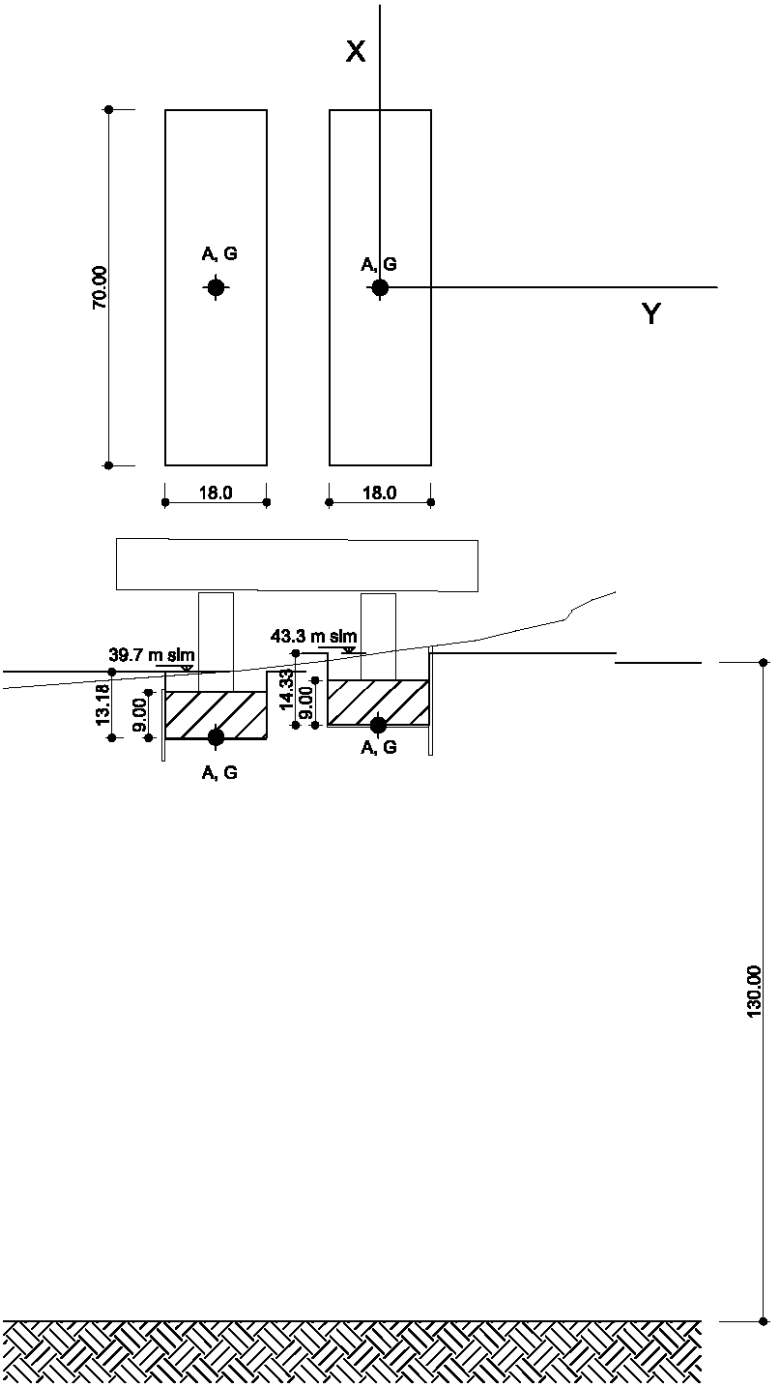

Figure 15. Foundations of the Calabria terminal structure.

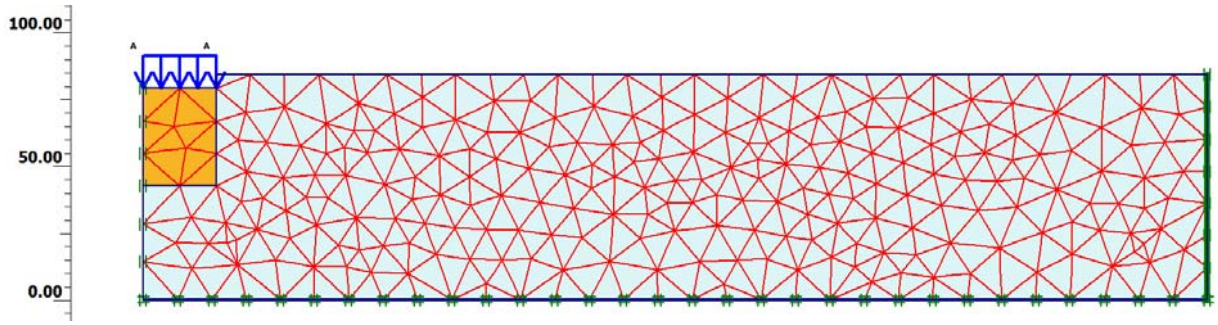

Figure 16. Finite element mesh used for the verification of the elastic solutions.

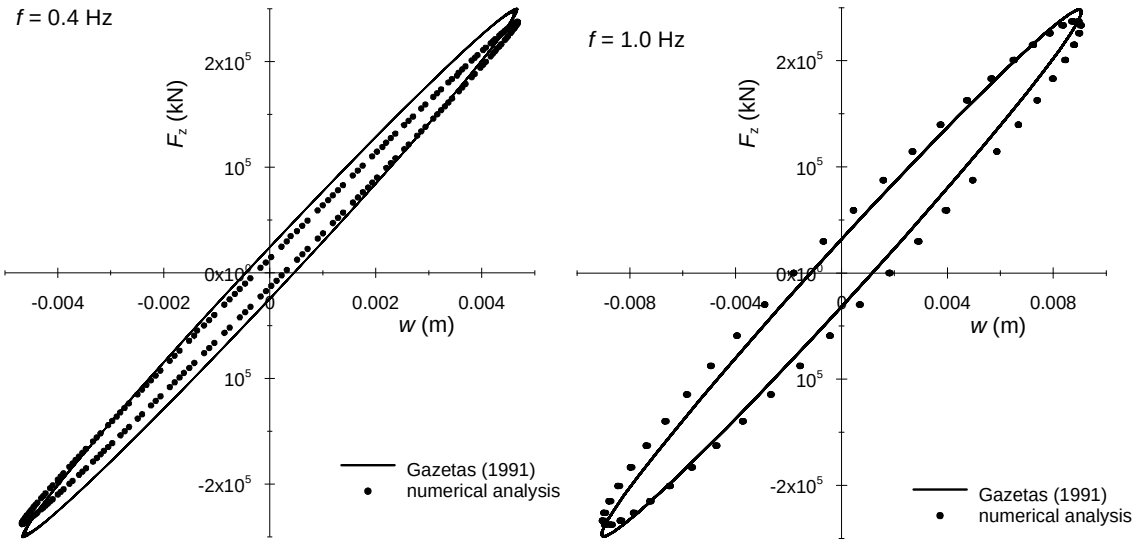

Figure 17.Comparison between the cyclic foundation response obtained from the simplified solutions by Gazetas (1991) and those resulting form the dynamic numerical analyses.

APPENDIX A

Details of the calculation of the dynamic impedance matrixes

SICILY TOWER single footing

radius	R	27.5	m	Soil density	0.002	Gg/m3
total area	Ab		m2			
distance	i	77.5	m			
embedment	D	41.5	m	loading frequency	0.35	Hz
	d	36.5	m	loading period	2.8	s
				ω	2.22	rad/s
thickness of layer	H	84	m	Vs	234.52	m/s
				ao = ωR/Vs	**0.26**	
hysteretic damping	ξ	**8.3**	%	H/R	3.1	
shear modulus	G	**110**	MPa	VLa	317.2637	m/s
Poisson's ratio	ν	0.2				
Young's modulus	E	264.0	MPa	fc	0.94	Hz
				fs	0.53	Hz

vertical displacement (z)

shallow circular found. on elastic layer	Kz(shallow-c)	21562.1	MN m		
dynamic coefficient	k(ω)	1			
radiation dashpot	C(ω)	0		f < fc	true
embedded foundation	Kz (emb-c)	5.29E+04	MN/m		
dynamic coefficient	k(ω)	1.01			
radiation dashpot	C(ω)	0			
dynamic stiffness	**Kz**	**5.33E+04**	**MN/m**	5.33E+07	kN/m
radiation dashpot	C(ω)	0			
hysteretic dashpot	Ch	3993	Gg/s		
Total dashpot	**C z**	**3993**	**Gg/s**	3.99E+06	Mg/s

torsion (rz)

shallow circular found. on elastic layer	Krz(shallow-c)	12600265.4	MN m		
dynamic coefficient	k(ω)	0.96			
radiation dashpot	C(ω)	---			
embedded circular found.	Krz(emb-c)	5.73E+07	MN m		
dynamic coefficient	k(ω)	0.96			
radiation dashpot	C(ω)	5.60E+02	Gg m^2 /s		
dynamic stiffness	**Kz**	**5.52E+07**	**MN m**	5.52E+10	kN m
radiation dashpot	C(ω)	5.60E+02	Gg m^2 /s		
hysteretic dashpot	Ch	4.13E+06	Gg m^2 /s		
Total dashpot	**C rz**	**4.13E+06**	**Gg m^2 /s**	4.13E+09	Mg m^2 /s

horizontal displacement (y) (longitudinal direction)

shallow circular found. on elastic layer	Ky(shallow-c)	15645.172	MN/m		
dynamic coefficient	k(ω)	---			
radiation dashpot	C(ω)	0		cy	0.9
				f < 0.75 fs	true
embedded foundation	Ky(emb-c)	5.89E+04	MN/m	f > 1.33 fs	false
dynamic coefficient	k(ω)	0.94			
dynamic stiffness	**Ky**	**5.54E+04**	**MN/m**	5.54E+07	kN/m
radiation dashpot	C(ω)	0			
hysteretic dashpot	Ch	4147	Gg/s		
Total dashpot	**C x**	**4147**	**Gg/s**	4.15E+06	Mg/s

horizontal displacement (x) (transversal direction)

shallow circular found. on elastic layer	Kx(shallow-c)	15645.172			
dynamic coefficient	k(ω)	---			
radiation dashpot	C(ω)	0		cx	0.9
				f < 0.75 fs	true
embedded foundation	Kx(emb-c)	5.89E+04	MN/m	f > 1.33 fs	false
dynamic coefficient	k(ω)	0.94			
dynamic stiffness	**Kx**	**5.54E+04**	**MN/m**	5.54E+07	kN/m
radiation dashpot	C(ω)	0			
hysteretic dashpot	Ch	4147	Gg/s		
Total dashpot	**C y**	**4147**	**Gg/s**	4.15E+06	Mg/s

rotation around x (rx)

shallow circular found. on elastic layer	Krx(shallow-c)	8049917.38	MN m		
dynamic coefficient	k(ω)	0.95			
radiation dashpot	C(ω)	0		f < fc	true
embedded circular found.	Krx(emb-c)	3.89E+07	MN m		
dynamic coefficient	k(ω)	0.95			
dynamic stiffness	**K rx**	**3.68E+07**	**MN m**	3.68E+10	kN m
radiation dashpot	C(ω)	0			
hysteretic dashpot	Ch	2759758	Gg m^2 /s		
Total dashpot	**C rx**	**2759758**	**Gg m^2 /s**	2.76E+09	Mg m^2 /s

rotation around y (ry)

shallow circular found. on elastic layer	Kry(shallow-c)	8049917.38			
dynamic coefficient	k(ω)	0.95			
radiation dashpot	C(ω)	0		f < fc	true
embedded circular found.	Kry(emb-c)	3.89E+07	MN m		
dynamic coefficient	k(ω)	0.95			
dynamic stiffness	**K ry**	**3.68E+07**	**MN m**	3.68E+10	kN m
radiation dashpot	C(ω)	0			
hysteretic dashpot	Ch	2759758	Gg m^2 /s		
Total dashpot	**C ry**	**2759758**	**Gg m^2 /s**	2.76E+09	Mg m^2 /s

mixed mode

circular y-rx	Ky-rx	7.17E+05	MN		
dynamic coefficient	k(ω)	1			
dynamic stiffness	**K y-rx**	**7.17E+05**	**MN/m**	7.17E+08	kN
radiation dashpot	C(ω)	0			
hysteretic dashpot	Ch	5.37E+04			
Total dashpot	**C y-rx**	**53671**	**Gg m /s**	5.37E+07	Mg m /s

mixed mode

circular x-ry	Kx-ry	7.17E+05	MN		
dynamic coefficient	k(ω)	1			
dynamic stiffness	**K x-ry**	**7.17E+05**	**MN/m**	7.17E+08	kN
radiation dashpot	C(ω)	0			
hysteretic dashpot	Ch	5.37E+04			
Total dashpot	**C x-ry**	**53671**	**Gg m /s**	5.37E+07	Mg m /s

CALABRIA TOWER single footing

radius	R	24 m	Soil density	0.002	Gg/m3
distance	i	78.45 m			
embedment	D	37 m	loading frequency	0.35	Hz
	d	32.5 m	loading period	2.8	s
			ω	2.22	rad/s
thickness of layer	H	100 m	Vs	567.89	m/s
			ao = ωR/Vs	**0.1**	
hysteretic damping	ξ	**2.3** %	H/R	4.2	
shear modulus	G	**645** MPa	VLa	768.2524	m/s
Poisson's ratio	ν	0.2			
Young's modulus	E	1548.0 MPa	fc	1.92	Hz
			fs	0.22	Hz

vertical displacement (z)

shallow circular found. on elastic layer	Kz(shallow-c)	101548.8	MN m	
dynamic coefficient	k(ω)	0.6		
radiation dashpot	C(ω)	0	f < fc	true
embedded foundation	Kz (emb-c)	2.21E+05	MN/m	
dynamic coefficient	k(ω)	0.60		
radiation dashpot	C(ω)	0		
dynamic stiffness	**Kz**	**1.33E+05**	**MN/m**	**1.33E+08 kN/m**
radiation dashpot	C(ω)	0		
hysteretic dashpot	Ch	2752	Gg/s	
Total dashpot	**C z**	**2752**	**Gg/s**	**2.75E+06 Mg/s**

torsion (rz)

shallow circular found. on elastic layer	Krz(shallow-c)	48695869.4	MN m	
dynamic coefficient	k(ω)	0.99		
radiation dashpot	C(ω)	---		
embedded circular found.	Krz(emb-c)	2.25E+08	MN m	
dynamic coefficient	k(ω)	0.99	ct	0.05
radiation dashpot	C(ω)	1.59E+02	Gg m^2 /s	c2 0.02
dynamic stiffness	**Kz**	**2.22E+08**	**MN m**	**2.22E+11 kN m**
radiation dashpot	C(ω)	1.59E+02	Gg m^2 /s	
hysteretic dashpot	Ch	4.60E+06	Gg m^2 /s	
Total dashpot	**C rz**	**4.60E+06**	**Gg m^2 /s**	**4.60E+09 Mg m^2 /s**

horizontal displacement (y) (longitudinal direction)

shallow circular found. on elastic layer	Ky(shallow-c)	77056	MN/m	
dynamic coefficient	k(ω)	---		
			cy	0.9
radiation dashpot	C(ω)∞	10.69	Gg/s	f < 0.75 fs false
				f > 1.33 fs true
embedded foundation	Ky(emb-c)	2.65E+05	MN/m	
dynamic coefficient	k(ω)	1.0		
dynamic stiffness	**Ky**	**2.65E+05**	**MN/m**	**2.65E+08 kN/m**
radiation dashpot	C(ω)	10.693		
hysteretic dashpot	Ch	5506	Gg/s	
Total dashpot	**C x**	**5.52E+03**	**Gg/s**	**5.52E+06 Mg/s**

horizontal displacement (x) (transversal direction)

shallow circular found. on elastic layer	Kx(shallow-c)	77056		
dynamic coefficient	k(ω)	---		
			cx	0.9
radiation dashpot	C(ω)∞	10.69	Gg/s	f < 0.75 fs false
				f > 1.33 fs true
embedded foundation	Kx(emb-c)	2.65E+05	MN/m	
dynamic coefficient	k(ω)	1.0		
dynamic stiffness	**Kx**	**2.65E+05**	**MN/m**	**2.65E+08 kN/m**
radiation dashpot	C(ω)	10.693		
hysteretic dashpot	Ch	5506	Gg/s	
Total dashpot	**C y**	**5517**	**Gg/s**	**5.52E+06 Mg/s**

rotation around x (rx)

	Ibx	521152.522	m4	
shallow circular found. on elastic layer	Krx(shallow-c)	30934241.3	MN m	
dynamic coefficient	k(ω)	0.98		
radiation dashpot	C(ω)	0	f < fc	true
embedded circular found.	Krx(emb-c)	1.42E+08	MN m	
dynamic coefficient	k(ω)	0.98		
dynamic stiffness	**Krx**	**1.40E+08**	**MN m**	**1.40E+11 kN m**
radiation dashpot	C(ω)	0		
hysteretic dashpot	Ch	2898233	Gg m^2 /s	
Total dashpot	**C rx**	**2898233**	**Gg m^2 /s**	**2.90E+09 Mg m^2 /s**

rotation around y (ry)

	Iby	521152.522	m4	
shallow circular found. on elastic layer	Kry(shallow-c)	30934241.3		
dynamic coefficient	k(ω)	0.98		
radiation dashpot	C(ω)	0	f < fc	true
embedded circular found.	Kry(emb-c)	1.42E+08	MN m	
dynamic coefficient	k(ω)	0.98		
dynamic stiffness	**Kry**	**1.40E+08**	**MN m**	**1.40E+11 kN m**
radiation dashpot	C(ω)	0		
hysteretic dashpot	Ch	2898233	Gg m^2 /s	
Total dashpot	**C ry**	**2898233**	**Gg m^2 /s**	**2.90E+09 Mg m^2 /s**

mixed mode

circular y-rx	Ky-rx	2.87E+06	MN	
dynamic coefficient	k(ω)	1		
dynamic stiffness	**Ky-rx**	**2.87E+06**	**MN/m**	**2.87E+09 kN**
radiation dashpot	C(ω)	0		
hysteretic dashpot	Ch	5.97E+04		
Total dashpot	**C y-rx**	**59653**	**Gg m /s**	**5.97E+07 Mg m /s**

mixed mode

circular x-ry	Kx-ry	2.87E+06	MN	
dynamic coefficient	k(ω)	1		
dynamic stiffness	**Kx-ry**	**2.87E+06**	**MN/m**	**2.87E+09 kN**
radiation dashpot	C(ω)	0		
hysteretic dashpot	Ch	5.97E+04		
Total dashpot	**C x-ry**	**59653**	**Gg m /s**	**5.97E+07 Mg m /s**

SICILY ANCHOR BLOCK

total area	Ab	11352	m2			
equivalent rectangle						
half-width	B	44	m			
half-length	L	64.5	m	loading frequency	2.00	Hz
	χ	0.682		loading period	0.5	s
				ω	12.57	rad/s
embedment	D	43.65	m			
	d	36	m	Vs	281.07	m/s
	Aw	15624	m2	$a_0 = \omega B/Vs$	**2.0**	
				H/R	0.0	
thickness of layer	H	145	m	VLa	380.2354	m/s
	B/H	0.303				
hysteretic damping	ξ	**5**	%	fc	0.66	Hz
shear modulus	G	**158**	MPa	fs	0.48	Hz
Poisson's ratio	ν	**0.2**				
Young's modulus	E	379.2	MPa	Soil density	0.002	Gg/m3

vertical displacement (z)

shallow rectangular found.	Kz (shallow-r)	60383.1	MN/m				
on elastic half-space	k(ω)	0.6		cz	1		
	C(ω)∞	9	Gg/s	f < fc	false		
radiation dashpot	C(ω)	7	Gg/s	f > 1.5 fc	true		
equivalent radius	Req(z)	60.8	m				
shallow circular found.	Kz(shallow-c)	74250.8	MN m				
on elastic layer							
embedded circular found.	Kz (emb-c)	1.26E+05	MN/m				
dynamic coefficient	k(ω)	0.80772579					
dynamic stiffness	**Kz**	**1.02E+05**	**MN/m**		**1.02E+08**	**kN/m**	
radiation dashpot	C(ω)	16	Gg/s				
hysteretic dashpot	Ch	809	Gg/s				
Total dashpot	**C z**	**8.25E+02**	**Gg/s**		**8.25E+05**	**Mg/s**	

torsion (rz)

polar moment of inertia	Ib=Ibx+Iby	19356817	m4				
shallow foundation	Krz(shallow-r)	184439994	MN m				
dynamic coefficient	k(ω)	0.72					
radiation dashpot	C(ω)	---					
equivalent radius	Req(rz)	60.3	m				
shallow circular found.	Krz(shallow-c)	1.92E+08	MN m	ct	0.7		
on elastic layer				c2	1.03		
embedded circular found.	Krz(emb-c)	4.99E+08	MN m		4.99E+11	kN m	
dynamic coefficient	k(ω)	0.72					
dynamic stiffness	**Kz**	**3.61E+08**	**MN m**		**3.61E+11**	**kN m**	
radiation dashpot	C(ω)	4.79E+04	Gg m^2 /s				
hysteretic dashpot	Ch	2.87E+06	Gg m^2 /s				
Total dashpot	**C rz**	**2.92E+06**	**Gg m^2 /s**		**2.92E+09**	**Mg m^2 /s**	

horizontal displacement (y)
(longitudinal direction)

shallow rectangular found.	Ky(shallow-r)	43098.0796	MN/m				
on elastic half-space	k(ω)	---		cy	1		
				f < 0.75 fs	false		
radiation dashpot	C(ω)∞	17	Gg/s	f > 1.33 fs	true		
equivalent radius	Req(y)	61.4	m				
shallow circular found.	Ky(shallow-c)	52219.0968	MN/m				
on elastic layer							
embedded circular found.	Ky(emb-c)	1.14E+05	MN/m				
dynamic coefficient	k(ω)	0.7					
dynamic stiffness	**Ky**	**7.98E+04**	**MN/m**		**7.98E+07**	**kN/m**	
radiation dashpot	C(ω)	28	Gg/s				
hysteretic dashpot	Ch	635	Gg/s				
Total dashpot	**C x**	**6.63E+02**	**Gg/s**		**6.63E+05**	**Mg/s**	

horizontal displacement (x)
(transversal direction)

shallow rectangular found.	Kx(shallow-r)	41920.2615					
on elastic half-space	k(ω)	---		cx	1		
				f < 0.75 fs	false		
radiation dashpot	C(ω)∞	16	Gg/s	f > 1.33 fs	true		
equivalent radius	Req(x)	59.7	m				
shallow circular found.	Kx(shallow-c)	50549.5581					
on elastic layer							
embedded circular found.	Kx(emb-c)	1.12E+05	MN/m				
dynamic coefficient	k(ω)	0.7					
dynamic stiffness	**Ky**	**7.81E+04**	**MN/m**		**7.81E+07**	**kN/m**	
radiation dashpot	C(ω)	28	Gg/s				
hysteretic dashpot	Ch	621	Gg/s				
Total dashpot	**C x**	**649**	**Gg/s**		**6.49E+05**	**Mg/s**	

rotation around x (rx)

moment of inertia	Ibx	8186419	m4				
shallow foundation	Krx(shallow-r)	9.12E+07	MN m				
dynamic coefficient	k(ω)	0.61					
	C(ω)∞	---		crx	0.5		
radiation dashpot	C(ω)	---		f < fc	false		
equivalent radius	Req(rx)	55.7	m				
shallow circular found.	Krx(shallow-c)	9.71E+07	MN m				
dynamic coefficient	k(ω)	0.61					
embedded circular found.	Krx(emb-c)	2.66E+08	MN m				
dynamic coefficient	k(ω)	0.61					
dynamic stiffness	**K rx**	**1.61E+08**	**MN m**		**1.61E+11**	**kN m**	
radiation dashpot	C(ω)	2.58E+07	Gg m^2 /s				
hysteretic dashpot	Ch	1.28E+06	Gg m^2 /s				
Total dashpot	**C rx**	**2.70E+07**	**Gg m^2 /s**		**2.70E+10**	**Mg m^2 /s**	

rotation around y (ry)

moment of inertia	Iby	11170398	m4				
shallow foundation	Kry(shallow-r)	1.21E+08	MN m				
dynamic coefficient	k(ω)	0.61					
	C(ω)∞	---		cry	0.5		
radiation dashpot	C(ω)	---		f < fc	false		
				c1	1.351913		
equivalent radius	Req(ry)	61.3	m				
shallow circular found.	Kry(shallow-c)	129954628	MN m				
on elastic layer		0.61					
embedded circular found.	Kry(emb-c)	3.38E+08	MN m				
dynamic coefficient	k(ω)	0.61					
dynamic stiffness	**K ry**	**2.05E+08**	**MN m**		**2.05E+11**	**kN m**	
radiation dashpot	C(ω)	4.17E+07	Gg m^2 /s				
hysteretic dashpot	Ch	1.63E+06	Gg m^2 /s				
Total dashpot	**C ry**	**4.33E+07**	**Gg m^2 /s**		**4.33E+10**	**Mg m^2 /s**	

mixed mode

circular y-rx	Ky-rx	2.41E+06	MN				
dynamic coefficient	k(ω)	1					
dynamic stiffness	**K y-rx**	**2.41E+06**	**MN/m**		**2.41E+09**	**kN**	
radiation dashpot	C(ω)	5.85E+02					
hysteretic dashpot	Ch	1.92E+04					
Total dashpot	**C y-rx**	**1.98E+04**	**Gg m /s**		**1.98E+07**	**Mg m /s**	

mixed mode

circular x-ry	Kx-ry	2.36E+06	MN				
dynamic coefficient	k(ω)	1					
dynamic stiffness	**K x-ry**	**2.36E+06**	**MN/m**		**2.36E+09**	**kN**	
radiation dashpot	C(ω)	5.85E+02					
hysteretic dashpot	Ch	1.88E+04					
Total dashpot	**C x-ry**	**1.94E+04**	**Gg m /s**		**1.94E+07**	**Mg m /s**	

CALABRIA ANCHOR BLOCK

total area	Ab	8950	m2			
equivalent rectangle						
half-width	B	44.75	m			
half-length	L	50	m	loading frequency	5.50	Hz
	χ	0.895		loading period	0.2	s
				ω	34.56	rad/s
embedment	D	37	m			
	d	37	m	Vs	779.10	m/s
	Aw	14023	m2	$a_0 = \omega B/Vs$	**2.0**	
				H/R	0.0	
thickness of layer	H	180	m	VLa	1053.983	m/s
	B/H	0.249				
hysteretic damping	ξ	**1.5**	%	fc	1.46	Hz
shear modulus	G	**1214**	MPa	fs	1.08	Hz
Poisson's ratio	ν	0.2				
Young's modulus	E	2913.6	MPa	Soil density	0.002	Gg/m3

vertical displacement (z)

shallow rectangular found.	Kz (shallow-r)	383881.9	MN/m				
on elastic half-space	k(ω)	0.6		cz	1		
	C(ω)∞	19	Gg/s	f < fc	false		
radiation dashpot	C(ω)	15	Gg/s	f > 1.5 fc	true		
equivalent radius	Req(z)	53.7	m				
shallow circular found.	Kz(shallow-c)	452123.3	MN m				
on elastic layer							
embedded circular found.	Kz (emb-c)	7.30E+05	MN/m				
dynamic coefficient	k(ω)	0.78447299					
dynamic stiffness	**Kz**	**5.72E+05**	**MN/m**		**5.72E+08**	**kN/m**	
radiation dashpot	C(ω)	37	Gg/s				
hysteretic dashpot	Ch	497	Gg/s				
Total dashpot	**C z**	**5.34E+02**	**Gg/s**		**5.34E+05**	**Mg/s**	

torsion (rz)

polar moment of inertia	Ib=Ibx+Iby	19356817	m4				
shallow foundation	Krz(shallow-r)	1417111872	MN m				
dynamic coefficient	k(ω)	0.72					
radiation dashpot	C(ω)	---					
equivalent radius	Req(rz)	60.3	m				
shallow circular found.	Krz(shallow-c)	1.46E+09	MN m	ct	0.7		
on elastic layer				c2	0.90		
embedded circular found.	Krz(emb-c)	3.87E+09	MN m		3.87E+12	kN m	
dynamic coefficient	k(ω)	0.72					
dynamic stiffness	**Krz**	**2.79E+09**	**MN m**		**2.79E+12**	**kN m**	
radiation dashpot	C(ω)	7.90E+04	Gg m^2 /s				
hysteretic dashpot	Ch	2.42E+06	Gg m^2 /s				
Total dashpot	**C rz**	**2.50E+06**	**Gg m^2 /s**		**2.50E+09**	**Mg m^2 /s**	

horizontal displacement (y)
(longitudinal direction)

shallow rectangular found.	Ky(shallow-r)	288327.893	MN/m				
on elastic half-space	k(ω)	---		cy	1		
				f < 0.75 fs	false		
radiation dashpot	C(ω)∞	40	Gg/s	f > 1.33 fs	true		
equivalent radius	Req(y)	53.4	m				
shallow circular found.	Ky(shallow-c)	331126.994	MN/m				
on elastic layer							
embedded circular found.	Ky(emb-c)	7.04E+05	MN/m				
dynamic coefficient	k(ω)	0.7					
dynamic stiffness	**Ky**	**4.93E+05**	**MN/m**		**4.93E+08**	**kN/m**	
radiation dashpot	C(ω)	66	Gg/s				
hysteretic dashpot	Ch	428	Gg/s				
Total dashpot	**C x**	**4.94E+02**	**Gg/s**		**4.94E+05**	**Mg/s**	

horizontal displacement (x)
(transversal direction)

shallow rectangular found.	Kx(shallow-r)	286010.256					
on elastic half-space	k(ω)	---		cx	1		
				f < 0.75 fs	false		
radiation dashpot	C(ω)∞	39	Gg/s	f > 1.33 fs	true		
equivalent radius	Req(x)	53.0	m				
shallow circular found.	Kx(shallow-c)	328124.068					
on elastic layer							
embedded circular found.	Kx(emb-c)	7.00E+05	MN/m				
dynamic coefficient	k(ω)	0.7					
dynamic stiffness	**Kx**	**4.90E+05**	**MN/m**		**4.90E+08**	**kN/m**	
radiation dashpot	C(ω)	66	Gg/s				
hysteretic dashpot	Ch	426	Gg/s				
Total dashpot	**C x**	**491**	**Gg/s**		**4.91E+05**	**Mg/s**	

rotation around x (rx)

moment of inertia	Ibx	8186419	m4				
shallow foundation	Krx(shallow-r)	6.80E+08	MN m				
dynamic coefficient	k(ω)	0.60					
	C(ω)∞	---		crx	0.5		
radiation dashpot	C(ω)	---		f < fc	false		
equivalent radius	Req(rx)	55.2	m				
shallow circular found.	Krx(shallow-c)	7.15E+08	MN m				
dynamic coefficient	k(ω)	0.60					
embedded circular found.	Krx(emb-c)	1.90E+09	MN m				
dynamic coefficient	k(ω)	0.60					
dynamic stiffness	**Krx**	**1.14E+09**	**MN m**		**1.14E+12**	**kN m**	
radiation dashpot	C(ω)	5.50E+07	Gg m^2 /s				
hysteretic dashpot	Ch	9.94E+05	Gg m^2 /s				
Total dashpot	**C rx**	**5.60E+07**	**Gg m^2 /s**		**5.60E+10**	**Mg m^2 /s**	

rotation around y (ry)

moment of inertia	Iby	11170398	m4				
shallow foundation	Kry(shallow-r)	8.94E+08	MN m				
dynamic coefficient	k(ω)	0.60					
	C(ω)∞	---		cry	0.5		
radiation dashpot	C(ω)	---		f < fc	false		
				c1	1.165765		
equivalent radius	Req(ry)	60.5	m				
shallow circular found.	Kry(shallow-c)	945463972	MN m				
on elastic layer		0.60					
embedded circular found.	Kry(emb-c)	2.38E+09	MN m				
dynamic coefficient	k(ω)	0.60					
dynamic stiffness	**Kry**	**1.44E+09**	**MN m**		**1.44E+12**	**kN m**	
radiation dashpot	C(ω)	6.27E+07	Gg m^2 /s				
hysteretic dashpot	Ch	1.25E+06	Gg m^2 /s				
Total dashpot	**C ry**	**6.39E+07**	**Gg m^2 /s**		**6.39E+10**	**Mg m^2 /s**	

SICILY TERMINAL STRUCTURE

total area	Ab	1260	m2			
equivalent rectangle						
half-width	B	9	m			
half-length	L	35	m	loading frequency	1.78	Hz
	χ	0.257		loading period	0.6	s
				ω	11.18	rad/s
embedment	D	27.1	m			
	d	25.6	m	Vs	220	m/s
	Aw	10624	m2	$a_0 = \omega B/Vs$	**0.5**	
				H/R	0.0	
thickness of layer	H	88.4	m	VLa	253	m/s
	B/H	0.102				
hysteretic damping	ξ	**9**	%	fc	2.47	Hz
shear modulus	G	**97**	MPa			
Poisson's ratio	ν	0.2				
Young's modulus	E	233.0	MPa	Soil density	0.002	Gg/m3

vertical displacement (z)

shallow rectangular found.	Kz (shallow-r)	12396.3	MN/m		
on elastic half-space	k(ω)	0.6		cz	1
	C(ω)∞	0	Gg/s	f < fc	true
radiation dashpot	C(ω)	0	Gg/s	f > 1.5 fc	false
equivalent radius	Req(z)	22.5	m		
shallow circular found.	Kz(shallow-c)	14543.6	MN m		
on elastic layer					
embedded circular found.	Kz (emb-c)	2.90E+04	MN/m		
dynamic coefficient	k(ω)	0.62829446			
dynamic stiffness	**Kz**	**1.82E+04**	**MN/m**	**1.82E+07**	**kN/m**
radiation dashpot	C(ω)	4	Gg/s		
hysteretic dashpot	Ch	297	Gg/s		
Total dashpot	**C z**	**3.01E+02**	**Gg/s**	**3.01E+05**	**Mg/s**

torsion (rz)

polar moment of inertia	Ib=Ibx+Iby	19356817	m4		
shallow foundation	Krz(shallow-r)	129296695	MN m		
dynamic coefficient	k(ω)	0.93			
radiation dashpot	C(ω)	---			
equivalent radius	Req(rz)	63.0	m		
shallow circular found.	Krz(shallow-c)	1.39E+08	MN m	ct	0.5
on elastic layer				c2	0.80
embedded circular found.	Krz(emb-c)	2.89E+08	MN m	2.89E+11	kN m
dynamic coefficient	k(ω)	0.93			
dynamic stiffness	**Krz**	**2.69E+08**	**MN/m**	**2.69E+11**	**kN m**
radiation dashpot	C(ω)	1.20E+03	Gg m^2 /s		
hysteretic dashpot	Ch	4.39E+06	Gg m^2 /s		
Total dashpot	**C rz**	**4.39E+06**	**Gg m^2 /s**	**4.39E+09**	**Mg m^2 /s**

horizontal displacement (y)
(longitudinal direction)

shallow rectangular found.	Ky(shallow-r)	10528.2232	MN/m		
on elastic half-space	k(ω)	---		cy	1
				f < 0.75 fs	false
radiation dashpot	C(ω)∞	3	Gg/s	f > 1.33 fs	true
equivalent radius	Req(y)	24.4	m		
shallow circular found.	Ky(shallow-c)	11980.9742	MN/m		
on elastic layer					
embedded circular found.	Ky(emb-c)	3.40E+04	MN/m		
dynamic coefficient	k(ω)	0.7			
dynamic stiffness	**Ky**	**2.38E+04**	**MN/m**	**2.38E+07**	**kN/m**
radiation dashpot	C(ω)	1819	Gg/s		
hysteretic dashpot	Ch	387	Gg/s		
Total dashpot	**C x**	**2.21E+03**	**Gg/s**	**2.21E+06**	**Mg/s**

horizontal displacement (x)
(transversal direction)

shallow rectangular found.	Kx(shallow-r)	9610.18683			
on elastic half-space	k(ω)	---		cx	1
				f < 0.75 fs	false
radiation dashpot	C(ω)∞	3	Gg/s	f > 1.33 fs	true
equivalent radius	Req(x)	22.3	m		
shallow circular found.	Kx(shallow-c)	10820.6308			
on elastic layer					
embedded circular found.	Kx(emb-c)	3.22E+04	MN/m		
dynamic coefficient	k(ω)	0.7			
dynamic stiffness	**Ky**	**2.25E+04**	**MN m**	**2.25E+07**	**kN/m**
radiation dashpot	C(ω)	1819	Gg/s		
hysteretic dashpot	Ch	366	Gg/s		
Total dashpot	**C x**	**2185**	**Gg/s**	**2.19E+06**	**Mg/s**

rotation around x (rx)

moment of inertia	Ibx	8186419	m4		
shallow foundation	Krx(shallow-r)	6.60E+07	MN m		
dynamic coefficient	k(ω)	0.90			
	C(ω)∞	---		crx	0.25
radiation dashpot	C(ω)	---		f < fc	true
equivalent radius	Req(rx)	58.8	m		
shallow circular found.	Krx(shallow-c)	7.34E+07	MN m		
dynamic coefficient	k(ω)	0.90			
embedded circular found.	Krx(emb-c)	1.65E+08	MN m		
dynamic coefficient	k(ω)	0.90			
dynamic stiffness	**Krx**	**1.49E+08**	**MN m**	**1.49E+11**	**kN m**
radiation dashpot	C(ω)	0	Gg m^2 /s		
hysteretic dashpot	Ch	2.42E+06	Gg m^2 /s		
Total dashpot	**C rx**	**2.42E+06**	**Gg m^2 /s**	**2.42E+09**	**Mg m^2 /s**

rotation around y (ry)

moment of inertia	Iby	11170398	m4		
shallow foundation	Kry(shallow-r)	8.63E+07	MN m		
dynamic coefficient	k(ω)	0.90			
	C(ω)∞	---		cry	0.5
radiation dashpot	C(ω)	---		f < fc	true
				c1	0.705931
equivalent radius	Req(ry)	64.4	m		
shallow circular found.	Kry(shallow-c)	96927430.4	MN m		
on elastic layer		0.90			
embedded circular found.	Kry(emb-c)	2.09E+08	MN m		
dynamic coefficient	k(ω)	0.90			
dynamic stiffness	**Kry**	**1.89E+08**	**MN m**	**1.89E+11**	**kN m**
radiation dashpot	C(ω)	0	Gg m^2 /s		
hysteretic dashpot	Ch	3.07E+06	Gg m^2 /s		
Total dashpot	**C ry**	**3.07E+06**	**Gg m^2 /s**	**3.07E+09**	**Mg m^2 /s**

mixed mode

circular y-rx	Ky-rx	2.90E+05	MN		
dynamic coefficient	k(ω)	1			
dynamic stiffness	**Ky-rx**	**2.90E+05**	**MN/m**	**2.90E+08**	**kN**
radiation dashpot	C(ω)	1.55E+04			
hysteretic dashpot	Ch	4.72E+03			
Total dashpot	**C y-rx**	**2.02E+04**	**Gg m /s**	**2.02E+07**	**Mg m /s**

mixed mode

circular x-ry	Kx-ry	2.75E+05	MN		
dynamic coefficient	k(ω)	1			
dynamic stiffness	**Kx-ry**	**2.75E+05**	**MN/m**	**2.75E+08**	**kN**
radiation dashpot	C(ω)	1.55E+04			
hysteretic dashpot	Ch	4.47E+03			
Total dashpot	**C x-ry**	**2.00E+04**	**Gg m /s**	**2.00E+07**	**Mg m /s**

CALABRIA TERMINAL STRUCTURE

total area	Ab	1260	m2			
equivalent rectangle						
half-width	B	9	m			
half-length	L	35	m	loading frequency	7.69	Hz
	χ	0.257		loading period	0.1	s
				ω	48.32	rad/s
embedment	D	13.75	m			
	d	9	m	Vs	595	m/s
	Aw	3735	m2	$a_0 = \omega B/Vs$	**1.7**	
				H/R	0.0	
thickness of layer	H	130	m	VLa	296	m/s
	B/H	0.069				
hysteretic damping	ξ	**2.2**	%	fc	8.23	Hz
shear modulus	G	**707**	MPa			
Poisson's ratio	ν	0.2				
Young's modulus	E	1696.8	MPa	Soil density	0.002	Gg/m3

vertical displacement (z)

shallow rectangular found.	Kz (shallow-r)	86836.1	MN/m			
on elastic half-space	k(ω)	0.6		cz	1	
	C(ω)∞	0	Gg/s	f < fc	true	
radiation dashpot	C(ω)	0	Gg/s	f > 1.5 fc	false	
equivalent radius	Req(z)	22.5	m			
shallow circular found.	Kz(shallow-c)	97467.9	MN m			
on elastic layer						
embedded circular found.	Kz (emb-c)	1.28E+05	MN/m			
dynamic coefficient	k(ω)	0.81588525				
dynamic stiffness	**Kz**	**1.05E+05**	**MN/m**	**1.05E+08**	**kN/m**	
radiation dashpot	C(ω)	2	Gg/s			
hysteretic dashpot	Ch	95	Gg/s			
Total dashpot	**C z**	**9.73E+01**	**Gg/s**	**9.73E+04**	**Mg/s**	

torsion (rz)

polar moment of inertia	Ib=Ibx+Iby	19356817	m4					
shallow foundation	Krz(shallow-r)	941429078	MN m					
dynamic coefficient	k(ω)	0.76						
radiation dashpot	C(ω)	---						
equivalent radius	Req(rz)	63.0	m					
shallow circular found.	Krz(shallow-c)	9.87E+08	MN m			ct	0.8	
on elastic layer						c2	1.21	
embedded circular found.	Krz(emb-c)	1.36E+09	MN m	1.36E+12	kN m			
dynamic coefficient	k(ω)	0.76						
dynamic stiffness	**Kz**	**1.04E+09**	**MN/m**	**1.04E+12**	**kN m**			
radiation dashpot	C(ω)	906.38	Gg m^2 /s					
hysteretic dashpot	Ch	9.45E+05	Gg m^2 /s					
Total dashpot	**C rz**	**9.46E+05**	**Gg m^2 /s**	**9.46E+08**	**Mg m^2 /s**			

horizontal displacement (y)
(longitudinal direction)

shallow rectangular found.	Ky(shallow-r)	76657.6086	MN/m			
on elastic half-space	k(ω)	---		cy	1	
				f < 0.75 fs	false	
radiation dashpot	C(ω)∞	2	Gg/s	f > 1.33 fs	true	
equivalent radius	Req(y)	24.4	m			
shallow circular found.	Ky(shallow-c)	83850.4468	MN/m			
on elastic layer						
embedded circular found.	Ky(emb-c)	1.30E+05	MN/m			
dynamic coefficient	k(ω)	0.7				
dynamic stiffness	**Ky**	**9.10E+04**	**MN/m**	**9.10E+07**	**kN/m**	
radiation dashpot	C(ω)	749	Gg/s			
hysteretic dashpot	Ch	83	Gg/s			
Total dashpot	**C x**	**8.32E+02**	**Gg/s**	**8.32E+05**	**Mg/s**	

horizontal displacement (x)
(transversal direction)

shallow rectangular found.	Kx(shallow-r)	69973.245						
on elastic half-space	k(ω)	---				cx	1	
						f < 0.75 fs	false	
radiation dashpot	C(ω)∞	1	Gg/s			f > 1.33 fs	true	
equivalent radius	Req(x)	22.3	m					
shallow circular found.	Kx(shallow-c)	75966.3762						
on elastic layer								
embedded circular found.	Kx(emb-c)	1.21E+05	MN/m					
dynamic coefficient	k(ω)	0.7						
dynamic stiffness	**Ky**	**8.45E+04**	**MN/m**	**8.45E+07**	**kN/m**			
radiation dashpot	C(ω)	749	Gg/s					
hysteretic dashpot	Ch	77	Gg/s					
Total dashpot	**C x**	**826**	**Gg/s**	**8.26E+05**	**Mg/s**			

rotation around x (rx)

moment of inertia	Ibx	8186419	m4			
shallow foundation	Krx(shallow-r)	4.80E+08	MN m			
dynamic coefficient	k(ω)	0.66				
	C(ω)∞	---		crx	0.5	
radiation dashpot	C(ω)	---		f < fc	true	
equivalent radius	Req(rx)	58.8	m			
shallow circular found.	Krx(shallow-c)	5.17E+08	MN m			
dynamic coefficient	k(ω)	0.66				
embedded circular found.	Krx(emb-c)	7.22E+08	MN m			
dynamic coefficient	k(ω)	0.66				
dynamic stiffness	**Krx**	**4.76E+08**	**MN/m**	**4.76E+11**	**kN m**	
radiation dashpot	C(ω)	0	Gg m^2 /s			
hysteretic dashpot	Ch	4.33E+05	Gg m^2 /s			
Total dashpot	**C rx**	**4.33E+05**	**Gg m^2 /s**	**4.33E+08**	**Mg m^2 /s**	

rotation around y (ry)

moment of inertia	Iby	11170398	m4					
shallow foundation	Kry(shallow-r)	6.28E+08	MN m					
dynamic coefficient	k(ω)	0.66						
	C(ω)∞	---				cry	0.75	
radiation dashpot	C(ω)	---				f < fc	true	
						c1	1.468516	
equivalent radius	Req(ry)	64.4	m					
shallow circular found.	Kry(shallow-c)	680873143	MN m					
on elastic layer		0.66						
embedded circular found.	Kry(emb-c)	9.31E+08	MN m					
dynamic coefficient	k(ω)	0.66						
dynamic stiffness	**Kry**	**6.14E+08**	**MN/m**	**6.14E+11**	**kN m**			
radiation dashpot	C(ω)	0	Gg m^2 /s					
hysteretic dashpot	Ch	5.59E+05	Gg m^2 /s					
Total dashpot	**C ry**	**5.59E+05**	**Gg m^2 /s**	**5.59E+08**	**Mg m^2 /s**			

mixed mode

circular y-rx	Ky-rx	3.90E+05	MN		
dynamic coefficient	k(ω)	1			
dynamic stiffness	**Ky-rx**	**3.90E+05**	**MN/m**	**3.90E+08**	**kN**
radiation dashpot	C(ω)	2.25E+03			
hysteretic dashpot	Ch	3.55E+02			
Total dashpot	**C y-rx**	**2.60E+03**	**Gg m /s**	**2.60E+06**	**Mg m /s**

mixed mode

circular x-ry	Kx-ry	3.62E+05	MN		
dynamic coefficient	k(ω)	1			
dynamic stiffness	**Kx-ry**	**3.62E+05**	**MN/m**	**3.62E+08**	**kN**
radiation dashpot	C(ω)	2.25E+03			
hysteretic dashpot	Ch	3.30E+02			
Total dashpot	**C x-ry**	**2.58E+03**	**Gg m /s**	**2.58E+06**	**Mg m /s**

APPENDIX B

Impedance solutions (Gazetas 1991)

TABLE 15.1 DYNAMIC STIFFNESSES AND DASHPOT COEFFICIENTS FOR ARBITRARILY SHAPED FOUNDATIONS ON THE SURFACE OF A HOMOGENEOUS HALFSPACE.

Vibration Mode	Dynamic Stiffness $\bar{K} = K \cdot k(\omega)$			Radiation Dashpot Coefficient C (General Shapes)
	Static Stiffness K		Dynamic Stiffness Coefficient k (General shape; $0 \leqslant a_0 \leqslant 2$)†	
	General Shape (foundation–soil contact surface is of area A_b and has a circumscribed rectangle $2L$ by $2B$; $L > B$)*	Square $L = B$		
Vertical, z	$K_z = \frac{2GL}{1-\nu}(0.73 + 1.54\chi^{0.75})$ with $\chi = \frac{A_b}{4L^2}$	$K_z = \frac{4.54GB}{1-\nu}$	$k_z = k_z\left(\frac{L}{B}, \nu; a_0\right)$ is plotted in Graph a	$C_z = (\rho V_{La} A_b) \cdot \tilde{c}_z$ $\tilde{c}_z = \tilde{c}_z(L/B, \nu; a_0)$ is plotted in Graph c
Horizontal, y (in the lateral direction)	$K_y = \frac{2GL}{2-\nu}(2 + 2.50\chi^{0.85})$	$K_y = \frac{9GB}{2-\nu}$	$k_y = k_y\left(\frac{L}{B}; a_0\right)$ is plotted in Graph b	$C_y = (\rho V_s A_b) \cdot \tilde{c}_y$ $\tilde{c}_y = \tilde{c}_y(L/B; a_0)$ is plotted in Graph d
Horizontal, x (in the longitudinal direction)	$K_x = K_y - \frac{0.2}{0.75-\nu} GL\left(1 - \frac{B}{L}\right)$	$K_x = K_y$	$k_x \simeq 1$	$C_x \simeq \rho V_s A_b$
Rocking, rx (around longitudinal x axis)	$K_{rx} = \frac{G}{1-\nu} I_{bx}^{0.75}\left(\frac{L}{B}\right)^{0.25}\left(2.4 + 0.5\frac{B}{L}\right)$ with I_{bx} (I_{by}) area moment of inertia of the foundation–soil contact surface around the x (y) axis	$K_{rx} = \frac{3.6GB^3}{1-\nu}$	$k_{rx} \simeq 1 - 0.20a_0$	$C_{rx} = (\rho V_{La} I_{bx}) \cdot \tilde{c}_{rx}$ $\tilde{c}_{rx} = \tilde{c}_{rx}(L/B; a_0)$ is plotted in Graphs e and f
Rocking, ry (around lateral axis)	$K_{ry} = \frac{G}{1-\nu} I_{by}^{0.75}\left[3\left(\frac{L}{B}\right)^{0.15}\right]$	$K_{ry} = K_{rx}$	$\begin{cases} \nu < 0.45: \\ k_{ry} \simeq 1 - 0.30a_0 \\ \nu \simeq 0.50: \\ k_{ry} \simeq 1 - 0.25a_0\left(\frac{L}{B}\right)^{0.30} \end{cases}$	$C_{ry} = (\rho V_{La} I_{by}) \cdot \tilde{c}_{ry}$ $\tilde{c}_{ry} = \tilde{c}_{ry}(L/B; a_0)$ is plotted in Graph g
Torsional	$K_t = GJ_b^{0.75}\left[4 + 11\left(1 - \frac{B}{L}\right)^{10}\right]$ with $J_b = I_{bx} + I_{by}$ being the polar moment of the soil–foundation contact surface	$K_t = 8.3GB^3$	$k_t \simeq 1 - 0.14a_0$	$C_t = (\rho V_s J_b) \cdot \tilde{c}_t$ $\tilde{c}_t = \tilde{c}_t(L/B; a_0)$ Graphs g

* Note that as $L/B \to \infty$ (strip footing) the theoretical values of K_z and $K_y \to 0$; the values computed from the two given formulas correspond to a footing with $L/B \approx 20$.

† $a_0 = \omega B / V_s$.

GRAPHS ACCOMPANYING TABLE 15.1

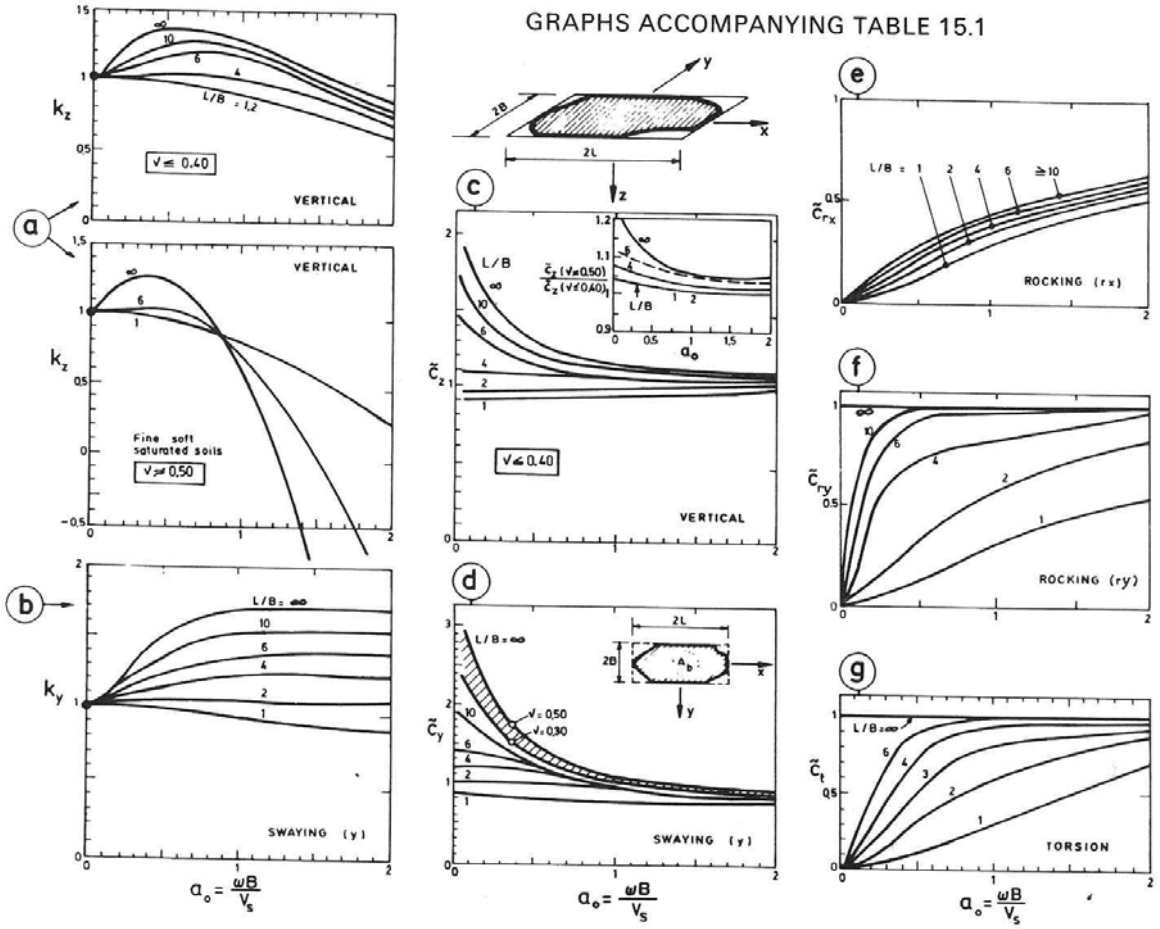

TABLE 15.2 DYNAMIC STIFFNESSES AND DASHPOT COEFFICIENTS FOR ARBITRARILY SHAPED PARTIALLY OR FULLY EMBEDDED IN A HOMOGENEOUS HALFSPACE.

Vibration Mode	*Dynamic Stiffness* $K_{emb} = K_{emb}(\omega)$		*Radiation Dashpot Coefficient* $C_{emb}(\omega)$	
	Static Stiffness K_{emb} For foundations with arbitrarily-shaped basemat A_b of circumscribed rectangle $2L$ by $2B$; total sidewall–soil contact area A_w (or constant sidewall–soil contact height d)	*Dynamic Stiffness Coefficient* $K_{emb}(\omega)$ $0 < a_0 \leq 2$	*General Foundation Shape*	*Rectangular Foundation* $2L$ *by* $2B$ *by* d
Vertical, z	$K_{z,emb} = K_{z,sur}\left[1 + \frac{1}{21}\frac{D}{B}(1 + 1.3\chi)\right] \times \left[1 + 0.2\left(\frac{A_w}{A_b}\right)^{2/3}\right]$ $K_{z,sur}$ obtained from Table 15.1 A_w = actual sidewall–soil contact area; for constant effective contact height d along the perimeter $A_w = (d) \times (\text{Perimeter})$; $\chi = A_b/4L^2$	Fully embedded: $K_{z,emb} \simeq K_{z,sur}\left[1 - 0.09\left(\frac{D}{B}\right)^{3/4} a_0^2\right]$ In a trench: $K_{z,tre} \simeq K_{z,sur}\left[1 + 0.09\left(\frac{D}{B}\right)^{3/4} a_0^2\right]$ Partially embedded: estimate by interpolating between the two $\nu \leq 0.40$ Fully embedded, $L/B = 1$–2 $K_{z,emb} \simeq 1 - 0.09\,(D/B)^{3/4} a_0^2$ Fully embedded, $L/B > 3$ $K_{z,emb} \simeq 1 - 0.35\,(D/B)^{1/2} a_0^{3.5}$ $\nu \geq 0.50$	$C_{z,emb} = C_{z,sur} + \rho V_s A_w$ with $C_{z,sur}$ and δ_z according to Table 15.1	$C_{z,emb} = 4\rho V_{La} B L \delta_z + 4\rho V_s (B + L) d$
Horizontal, y or x	$K_{y,emb} = K_{y,sur}\left(1 + 0.15\sqrt{\frac{D}{B}}\right) \times \left[1 + 0.52\left(\frac{h}{B}\frac{A_w}{L^2}\right)^{0.4}\right]$ $K_{y,sur}$ obtained from Table 15.1 $K_{x,emb}$ similarly computed from $K_{x,sur}$	$K_{y,emb}$ and $k_{s,emb}$ can be estimated in terms of L/B, D/B, and d/B for each value of a_0 from the graphs accompanying this table	$C_{y,emb} = C_{y,sur} + \rho V_s A_{ws} + \rho V_{La} A_{wse}$ $A_{ws} = \sum (A_w \sin \vartheta_i)$ = total effective sidewall area shearing the soil $A_{wse} = \sum (A_w \cos \vartheta_i)$ = total effective sidewall area compressing the soil ϑ_i angle of inclination of surface A_{wi} from loading direction $C_{y,sur}$ obtained from Table 15.1 $C_{x,emb}$ similarly computed from $C_{x,sur}$	$C_{y,emb} = 4\rho V_s B L \delta_y + 4\rho V_s B d + 4\rho V_{La} L d$ δ_y according to Table 15.1

	Expressions valid for any basemat shape but constant effective contact height d along the perimeter		$C_{rx,emb} = C_{rx,sur} + \rho V_{Ls} J_{wce} \tilde{c}_1$ $+ \rho V_s \left(J_{w_2} + \sum_i [A_{wce} \Delta_i^2] \right) \tilde{c}_1$ $\tilde{c}_1 = 0.25 + 0.65\sqrt{a_0} \left(\frac{d}{D}\right)^{-e_0/2} \times \left(\frac{D}{B}\right)^{-1/4}$ I_{wce} = total moment of inertia about their base axes parallel to x of all sidewall surfaces effectively compressing the soil Δ_i = distance of surface A_{wce_i} from the x axis J_{w_2} = polar moment of inertia about their base axes parallel to x of all sidewall surfaces effectively shearing the soil $C_{ry,emb}$ is similarly evaluated from $C_{ry,sur}$ with y replacing x and, in the equation for c_1, L replacing B	$C_{rx,emb} = \frac{4}{3}\rho V_{Ls} B^3 L \tilde{c}_{rx}$ $+ \frac{4}{3}\rho V_{Ls} d^3 L \tilde{c}_1$ $+ \frac{4}{3}\rho V_s B d (B^2 + d^2) \tilde{c}_1$ $+ 4\rho V_s B^2 d L \tilde{c}_1$ with $\tilde{c}_1$ as in the preceding column and $\tilde{c}_{rx}$ according to Table 15.1
Rocking, rx (around the longitudinal axis)	$K_{rx,emb} = K_{rx,sur}$ $\cdot \left\{1 + 1.26 \frac{d}{B}\left[1 + \frac{d}{B}\left(\frac{d}{D}\right)^{-0.2} \sqrt{\frac{B}{L}}\right]\right\}$	$k_{rx,emb} \simeq k_{rx,sur}$		
Rocking, ry (around the lateral axis)	$K_{ry,emb} = K_{ry,sur}$ $\cdot \left\{1 + 0.92\left(\frac{d}{L}\right)^{0.6}\left[1.5 + \left(\frac{d}{L}\right)^{1.9} \times \left(\frac{d}{D}\right)^{-0.6}\right]\right\}$	$k_{ry,emb} \simeq k_{ry,sur}$		
Coupling term Swaying–rocking (x, ry) Swaying–rocking (y, rx)	$K_{xry,emb} \simeq \frac{1}{3} d K_{x,emb}$ $K_{yrx,emb} \simeq \frac{1}{3} d K_{y,emb}$	$k_{rxy,emb} \simeq k_{yrx,emb} \simeq 1$	$C_{xry,emb} \approx \frac{1}{3} d C_{x,emb}$ $C_{yrx,emb} \approx \frac{1}{3} d C_{y,emb}$	as in the previous column
Torsional	$K_{t,emb} = K_{t,sur}$ $\times \left[1 + 1.4\left(1 + \frac{B}{L}\right)\left(\frac{d}{B}\right)^{0.9}\right]$	$k_{t,emb} \simeq k_{t,sur}$	$C_{t,emb} = C_{t,sur} + \rho V_{Ls} J_{wce} \tilde{c}_2$ $+ \rho V_s \sum [A_{wi} \Delta_{2i}^2] \tilde{c}_2$ $\tilde{c}_2 \approx \left(\frac{d}{D}\right)^{-0.5} \cdot \frac{a_0^2}{a_0^2 + \frac{1}{3}(L/B)^{-1.5}}$ J_{wce} = total moment of inertia of all sidewall surfaces effectively compressing the soil about the projection of the z axis onto their plane Δ_{2i} = distance of surface A_{wi} from the z axis	$C_{t,emb} = \frac{4}{3}\rho V_s BL (B^2 + L^2) \tilde{c}_t$ $+ \frac{4}{3}\rho V_{Ls} d (L^3 + B^3) \tilde{c}_2$ $+ 4\rho V_s dBL (B + L) \tilde{c}_2$ with $\tilde{c}_2$ as in the preceding column and $\tilde{c}_t$ according to Table 15.1

NOTE: $V_{Ls} = \frac{3.4}{\pi(1-\nu)} V_s$ is the apparent propagation velocity of compression–extension waves.

GRAPHS ACCOMPANYING TABLE 15.2

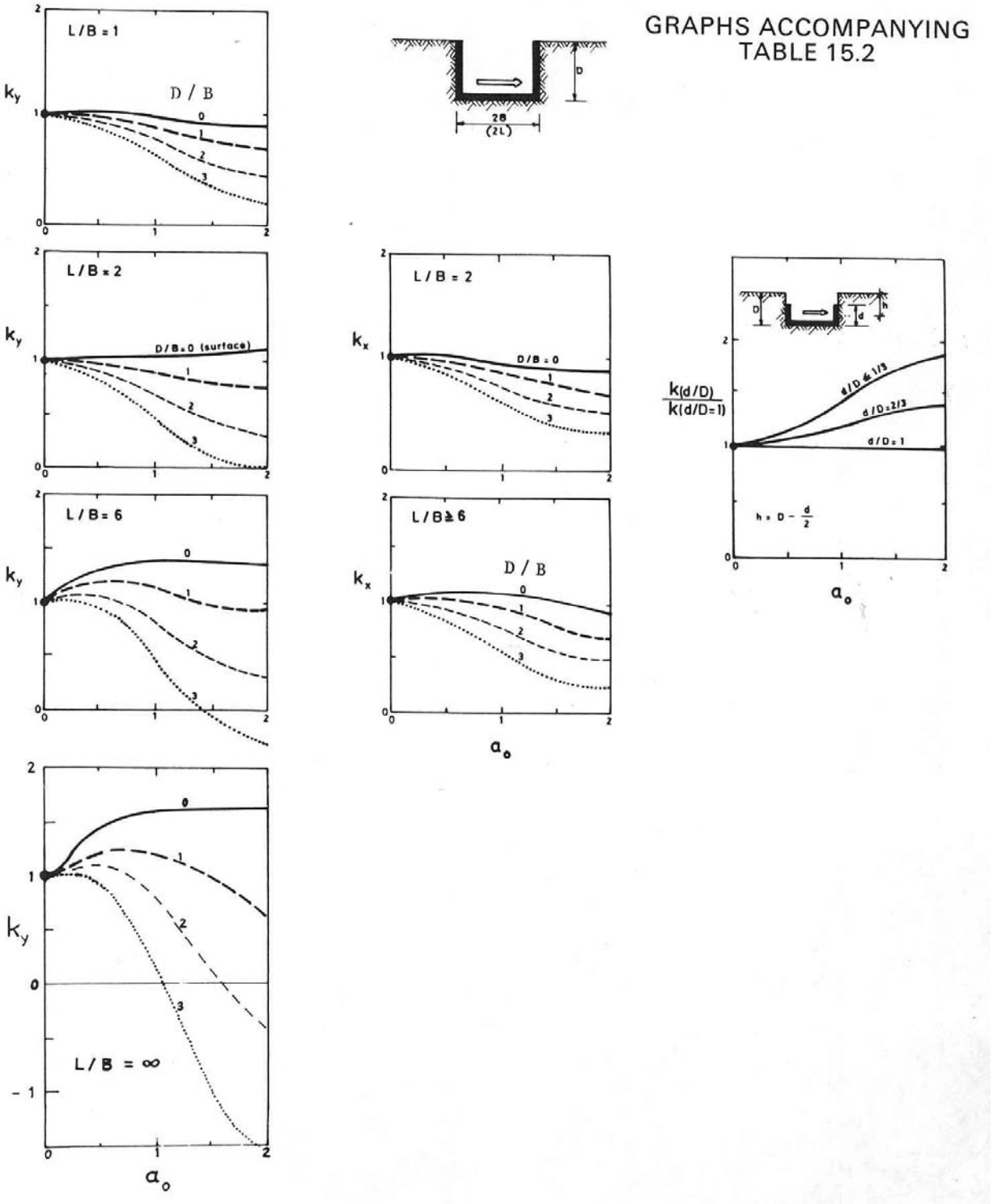

TABLE 15.3 DYNAMIC STIFFNESSES AND DASHPOT COEFFICIENTS FOR SURFACE FOUNDATIONS ON HOMOGENEOUS STRATUM OVER BEDROCK (sources are listed in the text).

	Foundation Shape	*Circular Foundation of Radius* $B = R$	*Rectangular Foundation* $2B$ *by* $2L$ $(L > B)$	*Strip Foundation* $2L \to \infty$
Static stiffnesses, K	Vertical, z	$K_z = \frac{4GR}{1-\nu}\left(1 + 1.3\frac{R}{H}\right)$	$K_z = \frac{2GL}{1-\nu}\left[0.73 + 1.54\left(\frac{B}{L}\right)^{3/4}\right]\left(1 + \frac{\frac{B}{H}}{0.5 + \frac{B}{L}}\right)$	$\frac{K_z}{2L} \simeq \frac{0.73G}{1-\nu}\left(1 + 3.5\frac{B}{H}\right)$
	Lateral, y	$K_y = \frac{8GR}{2-\nu}\left(1 + 0.5\frac{R}{H}\right)$	.	$\frac{K_y}{2L} \simeq \frac{2G}{2-\nu}\left(1 + 2\frac{B}{H}\right)$
	Lateral, x	$K_x = K_y$	.	—
	Rocking, rx	$K_{rx} = \frac{8GR^3}{3(1-\nu)}\left(1 + 0.17\frac{R}{H}\right)$	.	$\frac{K_{rx}}{2L} = \frac{\pi GB^2}{2(1-\nu)}\left(1 + 0.2\frac{B}{H}\right)$
	Rocking, ry	$K_{ry} = K_{rx}$	.	—
	Torsional, t	$K_t = \frac{16}{3}GR^3\left(1 + 0.10\frac{R}{H}\right)$	.	—
Dynamic stiffness coefficients, $k(\omega)$	Vertical, z	$k_z = k_z(H/R, a_0)$ is obtained from Graph III-1	$k_z = k_z(H/B, L/B, a_0)$ is plotted in Graph III-2 for rectangles and strip	
	Horizontal, y or x	$k_y = k_y(H/R, a_0)$ is obtained from Graph III-1	.	$k_y = k_y(H/B, a_0)$ is obtained from Graph III-3
	Rocking, rx or ry Torsional	$\left.\begin{matrix} k_\alpha(H/R) \simeq k_\alpha(\infty) \\ \alpha = rx, ry, t \end{matrix}\right\}$	.	$k_{rx}(H/R) \simeq k_{rx}(\infty)$
Radiation dashpot coefficients, $C(\omega)$	Vertical, z	$\left[\begin{matrix} C_z(H/B) \simeq 0 \text{ at frequencies } f < f_c, \text{ regardless of foundation shape} \\ C_z(H/B) \simeq 0.8C_z(\infty) \text{ at } f \geqslant 1.5f_c \\ \text{At intermediate frequencies: interpolate linearly.} \quad f_c = \frac{V_{La}}{4H}, \quad V_{La} = \frac{3.4V_s}{\pi(1-\nu)} \end{matrix}\right.$		
	Lateral, y or x	$\left[\begin{matrix} C_y(H/B) \simeq 0 \text{ at } f < \frac{1}{2}f_s; \quad C_y(H/B) \simeq C_y(\infty) \text{ at } f > \frac{1}{2}f_s \\ \text{At intermediate frequencies: interpolate linearly.} \quad f_s = V_s/4H. \text{ Similarly for } C_x \end{matrix}\right.$		
	Rocking, rx or ry	$C_{rx}(H/B) \simeq 0 \text{ at } f < f_c; \quad C_{rx}(H/B) \simeq C_{rx}(\infty) \text{ at } f > f_c$. Similarly for C_{ry}		
	Torsional, t	$C_t(H/B) \simeq C_t(\infty)$		

* Not available.

GRAPHS ACCOMPANYING TABLE 15.3

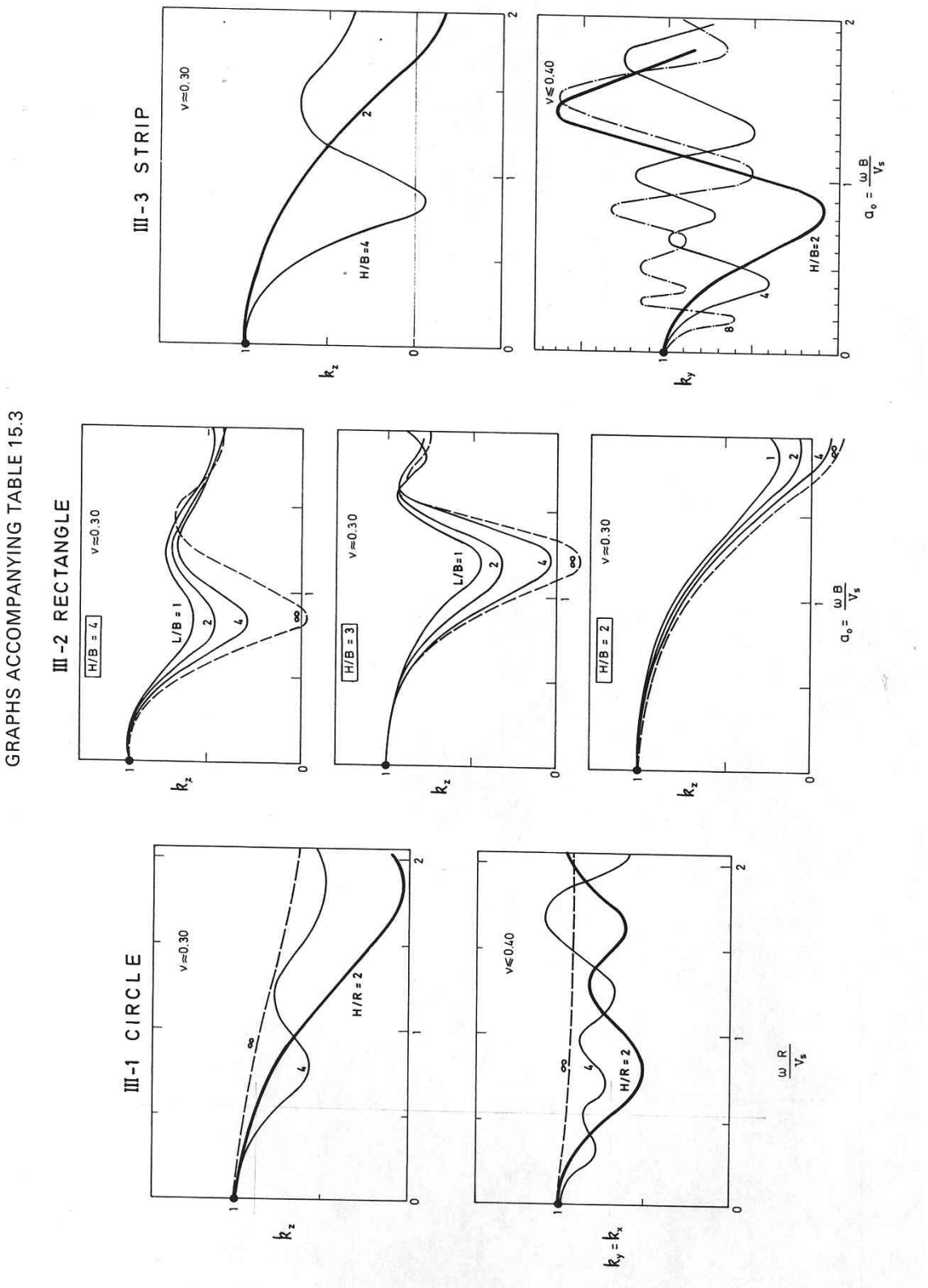

TABLE 15.4 DYNAMIC STIFFNESSES AND DASHPOT COEFFICIENTS FOR FOUNDATIONS EMBEDDED IN HOMOGENEOUS STRATUM OVER BEDROCK.*

Foundation Shape		Circular Foundation of Radius R	Strip Foundation
Static stiffnesses, K	Vertical	$K_{z,\text{emb}} \simeq K_{z,\text{sur}}\left(1+0.55\frac{d'}{R}\right)\left[1+\left(0.85-0.28\frac{D}{R}\right)\frac{D}{H-D}\right]^{\dagger}$	$K_{z,\text{emb}} \simeq K_{z,\text{sur}}\left[1+0.2\left(\frac{d'}{B}\right)^{2/3}\right]\left(1+3.5\frac{B}{H-D}\right)$
	Horizontal, y or x	$K_{y,\text{emb}} \simeq K_{y,\text{sur}}\left(1+\frac{d'}{R}\right)\left(1+1.25\frac{D}{H}\right)^{\dagger}$	$K_{y,\text{emb}} \simeq K_{y,\text{sur}}\left(1+0.5\frac{d'}{B}\right)\left(1+1.5\frac{D}{H}\right)$
	Rocking, rx or ry	$K_{rx,\text{emb}} \simeq K_{rx,\text{sur}}\left(1+2\frac{d}{R}\right)\left(1+0.65\frac{D}{H}\right)$	$K_{rx,\text{emb}} \simeq K_{rx,\text{sur}}\left(1+\frac{d'}{B}\right)\left(1+0.65\frac{D}{H}\right)$
	Coupled sweaying–rocking	$K_{yrx,\text{emb}} \simeq \frac{1}{3}dK_{y,\text{emb}}$	$K_{yrx,\text{emb}} \simeq \frac{1}{3}dK_{y,\text{emb}}$
	Torsional	$K_{t,\text{emb}} \simeq K_{t,\text{sur}}\left(1+2.67\frac{d'}{R}\right)$	—
Dynamic stiffness coefficients, $k(\omega)$		The relationships between k_{emb} and k_{sur} follow approximately the same pattern as those between embedded and surface foundation on a homogeneous halfspace. Therefore, use the results of Table 15.2 as a first approximation.	
Radiation dashpot coefficients, $C(\omega)$		C_{emb} exceeds C_{sur} by an amount that depends on the geometry of the sidewall–soil contact surface and is practically independent of the presence or absence of a rigid base at shallow depths. Therefore, use the results of Table 15.2, but with C_{sur} corresponding to the layered profile and thus obtained according to Table 15.3 (approximate guideline).	

* Sources are listed in the text.
† $K_{z,\text{sur}}$, $K_{y,\text{sur}}$, . . . are the stiffnesses for the corresponding surface foundations, and can be obtained from Table 15.3.